ISSN: 2754-4966

Journal of Nanosciences Research & Reports

SCIENTIFIC Research and Community

Research Article

Open Access

# A Bioorthogonal Strategy for Preparing BMP4-Associated Hemp-Derived Extracellular Vesicle Preparations: Comparative Evaluation of Reaction Conditions and Physicochemical Characterization

**Hamid Moloudian[1,2], Nasser Nassiri Koopaei[3], FNU Joshua[1,2], Ibrokhim D. Lutfullaev[4], Brent A. Reynolds[5†], Hassan Azari[6*] and Lei Zhai[1,2*]**

[1]NanoScience Technology Center, University of Central Florida, Orlando, FL 32826, USA

[2]Department of Chemistry, University of Central Florida, Orlando, FL 32816, USA

[3]EriVan Bio, Gainesville, FL 32615, USA

[4]College of Osteopathic Medicine, Pacific Northwest University of Health Sciences, Yakima, WA 98901, USA

[5]Department of Neurosurgery, University of Florida, Gainesville, FL 32608, USA

[6]College of Health Professions and Medical Sciences, Barry University, Miami Shores, FL 33161, USA

[†]Deceased on April 11, 2026

## ABSTRACT

Plant-derived extracellular vesicle (PEV) preparations are promising bio-derived platforms for therapeutic cargo association, although controlled modification of heterogeneous PEV preparations remains challenging. Here, a proof-of-concept evaluation of a two-component dibenzocyclooctyne (DBCO)/azide workflow was performed for preparing bone morphogenetic protein 4 (BMP4)-associated hemp-derived extracellular vesicle (HEV) preparations under mild, strain-promoted azide–alkyne cycloaddition-compatible conditions. Purified native HEV preparations were characterized by nanoparticle tracking analysis and transmission electron microscopy, supporting predominantly nanoscale particle populations with vesicle-like morphology. Fluorescamine-accessible primary amines were quantified to define nominal DBCO-reagent-to-amine feed conditions, and DBCO-responsive behavior was compared using a 9-(azidomethyl) anthracene (Anth-$N_3$) fluorescence assay. At a nominal feed ratio of 4.5, apparent DBCO-responsive conversion metrics were 13.0 ± 0.64% at pH 7.4 and 18.3 ± 2.74% at pH 8.5, whereas exploratory higher-feed conditions (~30–50) produced values around 12%. Following incubation of DBCO-treated HEVs with azide-reagent-treated BMP4 and purification, enzyme-linked immunosorbent assay (ELISA) showed particle-normalized BMP4 association of approximately 1.60 and 6.66 pg per $10^9$ particles at pH 7.4 and 8.5, respectively, compared with approximately 0.04–0.60 pg per $10^9$ particles for exploratory high-feed preparations. Nano-flow cytometry further detected fluorescence associated with fluorescein-labeled BMP4 within membrane-dye-positive particle populations. For the Anth-$N_3$-responsive and particle-normalized ELISA readouts, the lower-feed pH 8.5 condition was most favorable among those evaluated. The before recovered materials are conservatively described as BMP4-associated HEV preparations because the analytical workflow was comparative rather than bond-specific. These findings support continued development and more comprehensive validation of bioorthogonal protein-association strategies for PEV preparations.

***Corresponding authors**

Hassan Azari, College of Health Professions and Medical Sciences, Barry University, Miami Shores, FL 33161, USA. Email: hazari@barry.edu

Lei Zhai, NanoScience Technology Center, Department of Chemistry, University of Central Florida, Orlando, FL 32816, USA. Email: lzhai@ucf.edu

**Received:** October 09, 2026; **Accepted:** October 15, 2026; **Published:** October 31, 2026

**Keywords:** Glioblastoma Multiforme, Bone Morphogenetic Protein 4 (BMP4), Hemp-derived Extracellular Vesicles (HEVs), Plant-derived Nanocarriers, Bioorthogonal Chemistry, Strain-Promoted Azide–Alkyne Cycloaddition (SPAAC)

**Abbreviations**

Anth-Cl 9-(chloromethyl)anthracene
Anth-$N_3$ 9-(azidomethyl)anthracene
BCA bicinchoninic acid
BMP4 bone morphogenetic protein 4
BMP4FITC fluorescein isothiocyanate-labeled bone morphogenetic protein 4
DBCO dibenzocyclooctyne
DI deionized
DLS dynamic light scattering
DMSO dimethyl sulfoxide
ELISA enzyme-linked immunosorbent assay
EV extracellular vesicle
FITC fluorescein isothiocyanate
GBM glioblastoma
HEV hemp-derived extracellular vesicle
MWCO molecular weight cutoff
NanoFCM nano-flow cytometry
NHS N-hydroxysuccinimide
NTA nanoparticle tracking analysis
PBS phosphate-buffered saline

PEG poly(ethylene glycol)
PEV plant-derived extracellular vesicle
PFA paraformaldehyde
SPAAC strain-promoted azide–alkyne cycloaddition
TEM transmission electron microscopy

## Introduction

Glioblastoma (GBM) is the most common malignant primary brain tumor in adults and remains associated with poor survival despite treatment combining surgical resection, radiotherapy, and chemotherapy [1]. Its management is complicated by diffuse infiltration, extensive cellular heterogeneity, treatment-resistant stem-like populations, and limited delivery of many therapeutics across the blood–brain barrier [2,3]. These challenges have motivated strategies that act on tumor-initiating cells while supporting therapeutic delivery to dispersed tumor regions.

Bone morphogenetic protein 4 (BMP4), a member of the transforming growth factor-β superfamily, has been investigated as a differentiation-based therapeutic agent for GBM [4]. In patient-derived GBM models, BMP4-mediated activation of BMP receptor/Smad signaling reduced proliferation and clonogenicity, decreased tumor-initiating populations, and promoted a more differentiated phenotype [5,6]. BMP4 also reduced tumor initiation, invasion, and intracranial tumor growth in preclinical studies [5,7,8]. A first-in-human phase 1 study further indicated that local administration of recombinant human BMP4 by convection-enhanced delivery was feasible and generally well tolerated in patients with recurrent GBM [9]. Broader translation nevertheless remains limited by the pharmacokinetic behavior of therapeutic proteins and the difficulty of distributing them throughout infiltrative brain tumors [8,10].

Extracellular vesicles (EVs) are lipid-bilayer-enclosed particles involved in intercellular transport and have attracted interest as carriers for therapeutic biomolecules [11–14]. Plant-derived extracellular vesicle (PEV) preparations may offer renewable sourcing, scalability, and relatively economical production [15–18]. Hemp (*Cannabis sativa* L.)-derived EV (HEV) preparations have been reported to contain phytocannabinoids and to induce cell-cycle arrest and apoptosis in hepatocellular carcinoma cells [19], supporting their investigation as intrinsically bioactive nanomaterials. HEV preparations have also shown anti-inflammatory and barrier-protective effects in a preclinical colitis model [20]. In preliminary GBM studies, HEVs reduced glioma-cell viability and migration in vitro and, following intranasal administration, were distributed throughout tumor-bearing brains, including the tumor core [21]. However, PEV preparations can be compositionally heterogeneous and may contain diverse biomolecules and co-isolated material, complicating chemical modification, purification, and fluorescence-based analysis [15–18].

Association of therapeutic proteins with EVs requires reaction conditions compatible with both the protein and the vesicle preparation. Direct amine-reactive coupling may produce heterogeneous products because nucleophilic groups are present on both the vesicle preparation and the therapeutic protein, potentially promoting uncontrolled crosslinking or exposing the protein to vesicle-treatment conditions. Strain-promoted azide–alkyne cycloaddition (SPAAC) offers a modular alternative in which complementary azide and strained-alkyne groups are introduced separately and subsequently reacted under mild, copper-free conditions [22–24]. This design allows the vesicle and protein components to be treated and purified separately and limits direct exposure of the protein to the HEV-treatment conditions. Dibenzocyclooctyne–N-hydroxysuccinimidyl (DBCO–NHS)-based surface modification has previously been applied to EVs derived from mammalian cells, including plasma-, mesenchymal stromal cell-, microglial-, and other cell-derived EV preparations, followed by coupling to azide-bearing fluorophores, peptides, proteins, or targeting ligands [25–28]. Related DBCO/azide strategies have also been used with synthetic lipid vesicles [28]. These studies establish the chemical feasibility of DBCO-mediated SPAAC modification across multiple vesicular systems, whereas systematic application to PEV preparations remains comparatively limited.

Selected non-optimized observations from the present HEV-BMP4 workflow were previously disclosed in a review from our group [29]. The present study extends that initial report through a comparative, chemistry-focused proof-of-concept evaluation of nominal DBCO-PEG4-NHS-to-amine feed conditions and reaction pH. Fluorescamine-accessible amine equivalents and anthracene-azide (Anth-$N_3$)-responsive fluorescence were evaluated, while post-purification BMP4 or fluorescein isothiocyanate-labeled BMP4 (BMP4FITC) association was assessed using enzyme-linked immunosorbent assay (ELISA), nano-flow cytometry (NanoFCM), and complementary bulk fluorescence analysis. The recovered materials were evaluated as BMP4- or BMP4FITC-associated HEV preparations rather than as definitively established covalent conjugates. By linking HEV-treatment conditions with post-purification protein recovery across complementary analytical readouts, the study provides a foundational framework for the further development and validation of bioorthogonal protein-association strategies for HEV preparations. The present study is therefore positioned as a chemistry-focused evaluation of reaction conditions and workflow feasibility rather than a comprehensive validation of covalent coupling.

## Materials and Methods

### Materials

Fluorescamine (Thermo Scientific, Cat. No. 043749.ME, ≥98.0%) and 1-hexylamine (Thermo Scientific, Cat. No. A15663.AK, ≥98.5%) were used for the measurement of fluorescamine-accessible primary amines in HEV preparations. DBCO-$PEG_4$-NHS ester (BroadPharm, Cat. No. BP-22288, 98%) and azide-$PEG_6$-NHS ester (Lumiprobe, Cat. No. 3692-1g, ≥95%) were used for chemical treatment of HEVs and BMP4, respectively. Recombinant human BMP4 produced in *Escherichia coli* (R&D Systems, Cat. No. 314-BPE-010, >95%) and FITC-labeled, His-tagged recombinant human BMP4 (BMP4FITC; Aviscera Bioscience, Cat. No. 00014-01-50F, >90%) were used in protein-treatment and HEV-association experiments. BMP4 in purified HEV-containing preparations was measured using the Quantikine Human BMP4 ELISA kit (R&D Systems, Cat. No. DBP400). MemGlow 640 membrane-labeling dye (Cytoskeleton, Cat. No. MG04) was used for NanoFCM fluorescence phenotyping, and an S16M-Exo silica nanoparticle standard mixture was used for NanoFCM size calibration. Dialysis membranes with molecular-weight cutoffs (MWCOs) of 3.5 kDa (Thermo Fisher Scientific, Cat. No. 88242) and 100 kDa (Fisher Scientific, Cat. No. 08-700-132) were used during purification. Fresh female inflorescences of *Cannabis sativa* L. (hemp) labeled as the 'Lemon Zest' cultivar and containing less than 0.3% tetrahydrocannabinol were obtained from a local farm in Central Florida, USA. HEVs isolated from this material were supplied by the collaborating organization, EriVan Bio (Gainesville, FL, USA). Phosphate-buffered saline (PBS), anhydrous dimethyl sulfoxide (DMSO), sodium chloride, sodium hydroxide, hydrochloric acid, sucrose, paraformaldehyde (PFA), glutaraldehyde, uranyl acetate, borate buffer, and deionized (DI) water were used as described in the corresponding methods.

Formvar–carbon-coated grids were used for transmission electron microscopy (TEM). Unless otherwise specified, reagents and solvents were of analytical grade and used as received.

**Isolation and Purification of Native HEVs**

HEVs supplied by EriVan Bio (Gainesville, FL, USA) were isolated and purified from the hemp material using the following procedure [30]. Fresh hemp inflorescences (20 g), with woody material and stems removed, were rinsed twice with DI water at approximately 22 °C to remove surface particulates. The plant material was suspended in 200 mL of 4 °C PBS and homogenized using a high-shear masticator system in three 1-min cycles separated by 30-s rest periods to limit heating. The crude homogenate was clarified by sequential centrifugation at 4 °C. Samples were centrifuged at 1,000 ×g for 30 min, followed by transfer of the supernatant to a fresh tube and centrifugation at 3,000 ×g for 30 min. The resulting supernatant was then centrifuged at 10,000 ×g for 1 h to remove larger particles and insoluble material. The recovered supernatant was sequentially filtered through 0.45- and 0.22-µm membrane filters and ultracentrifuged at 120,000 ×g for 90 min using an SW28 swinging-bucket rotor. The pellet was washed once with cold PBS and resuspended in 1–2 mL of PBS. For density-based purification, the resuspended preparation was loaded onto a discontinuous sucrose gradient containing 8%, 15%, 30%, 45%, and 60% (w/v) sucrose layers prepared in PBS. The gradient was centrifuged at 145,000 ×g for 120 min at 4 °C. Material collected from the 30%–45% sucrose interface was diluted with PBS and recovered by a final ultracentrifugation step at 120,000 ×g for 90 min at 4 °C. The final HEV preparation was resuspended in calcium- and magnesium-free PBS and stored at −80 °C until use. Physicochemical characterization of the purified native HEV preparation was performed as described below.

**Nanoparticle Tracking Analysis**

Nanoparticle tracking analysis (NTA) was used for baseline characterization of the particle concentration and size distribution of the purified native HEV preparation [30,31]. HEV suspensions were diluted in calcium- and magnesium-free PBS to obtain a concentration suitable for single-particle tracking. Preliminary dilution factors ranging from 1:100 to 1:65,000 were evaluated to identify an appropriate working concentration. Measurements were performed using a NanoSight NS300 instrument (Malvern Panalytical, UK) at 22 °C, and videos were analyzed using NTA software version 3.4. Three 60-s videos were acquired from the same native HEV preparation and treated as technical acquisitions rather than independent biological replicates. The resulting particle tracks were used to determine the concentration and hydrodynamic size distribution of the native preparation, including the mean, mode, median diameter (D50), D10, and D90 values. Where stock concentration was reported, the measured concentration of the diluted sample was corrected using the experimentally applied dilution factor. NTA and NanoFCM were both used to characterize native HEVs. NTA provided the baseline particle concentration and hydrodynamic size distribution and was used to normalize the BCA-detectable protein content of the initial preparation, as described in Supplementary Information (SI). NTA, TEM, and NanoFCM characterization were not performed on the same native HEV batch. Accordingly, particle-size values obtained by these methods were treated as batch- and method-specific characterization measurements rather than as directly interchangeable estimates of an identical preparation.

**TEM and Morphometric Analysis**

Purified native HEV suspensions in PBS were gently mixed for 30 s and combined at a 1:1 volume ratio with 4% PFA in PBS to obtain a final PFA concentration of 2%. Aliquots of 10–20 µL were placed on Parafilm, and Formvar–carbon-coated grids were floated on the sample droplets for 20 min. The grids were washed with PBS, post-fixed with 1% glutaraldehyde in PBS for 5 min, rinsed with DI water for 2 min, and negatively stained with 4% aqueous uranyl acetate for 10 min [31]. After air-drying at room temperature for 5–10 min, the grids were examined using a Tecnai G2 F20-TWIN TEM. Apparent diameters of selected vesicle-like structures were measured manually from multiple TEM micrographs. Structures were included when they showed a discrete, approximately rounded boundary that could be distinguished from surrounding irregular or electron-dense material. Apparent diameters were reported as mean ± standard deviation and observed range.

**Quantification of Fluorescamine-Accessible Primary Amines in HEV Preparations**

Fluorescamine-accessible primary amines in HEV preparations were quantified using a fluorescamine assay with 1-hexylamine as the calibration standard [28]. A fresh fluorescamine solution was prepared at 0.3 mg $mL^{-1}$ in anhydrous DMSO and protected from light. 1-Hexylamine standards ranging from 0 to 0.30 mM were prepared in DI water. For each standard, 25 µL of 1-hexylamine solution was combined with 725 µL of 0.1 M borate buffer (pH 9.5) and 250 µL of fluorescamine solution. HEV samples were analyzed under the same conditions by replacing the 1-hexylamine standard with 25 µL of HEV dispersion. The mixtures were vortexed for 30 s. Immediately thereafter, 100 µL aliquots were transferred to a clear, flat-bottom 96-well plate, and fluorescence was measured using a Tecan Infinite M200 Pro microplate reader (Tecan, Switzerland) at excitation and emission wavelengths of 410 and 470 nm, respectively. Calibration standards were measured in triplicate as technical replicates. HEV-associated fluorescence values were converted to 1-hexylamine-equivalent primary amine concentrations using the calibration curve and corrected for sample dilution, where applicable. Because the assay detects only primary amines accessible to fluorescamine under the applied reaction conditions, the results were interpreted as fluorescamine-accessible primary amine equivalents.

**Preparation of DBCO-Treated HEVs**

The treatment strategy was adapted from previously reported vesicle-functionalization approaches [27,28]. HEVs were treated with DBCO-$PEG_4$-NHS ester through an NHS ester–amine reaction (Figure 1). A concentrated DBCO-$PEG_4$-NHS ester stock solution was prepared by dissolving 178.6 mg of the reagent in 1.00 mL of anhydrous DMSO (275 mM). Reaction conditions were defined using nominal molar feed ratios of DBCO-$PEG_4$-NHS ester to fluorescamine-accessible primary amine equivalents in the HEV preparation. These ratios were calculated from fluorescamine-derived 1-hexylamine-equivalent concentrations and therefore represent reagent-input conditions rather than measured degrees of HEV modification. Exploratory preparations employed nominal DBCO-to-amine feed ratios of approximately 30–50 at pH 8.0–9.0, whereas subsequent preparations were performed at a lower nominal feed ratio of 4.5 at pH 7.4 or 8.5. Depending on the preparation, 5–15 µL of the DBCO-$PEG_4$-NHS stock solution was added to 0.5–3.0 mL of HEV stock dispersion, in glass vials. Batch-specific particle concentrations and fluorescamine-derived amine-equivalent concentrations were used to define the nominal DBCO-to-amine feed conditions. The reaction pH was adjusted using 0.1 M sodium hydroxide or 0.1 M hydrochloric acid and monitored during incubation. The mixtures were incubated overnight at 4–8 °C with orbital agitation. Following incubation, the preparations were dialyzed against 1 L of 0.9% (w/v) sodium chloride at 4–8 °C using a 3.5-kDa MWCO

membrane to reduce unreacted DBCO-PEG$_4$-NHS ester, DMSO, and other low-molecular-weight reaction components. Three buffer exchanges were performed, each lasting approximately 2–4 h. The recovered preparations, hereafter termed DBCO-treated HEVs, were transferred to microcentrifuge tubes and used for subsequent characterization and reaction with azide-reagent-treated BMP4 or BMP4FITC.

### Assessment of DBCO-Responsive Fluorescence Using the Anth-$N_3$ Assay

The Anth-$N_3$ assay was adapted from previously reported post-assembly vesicle-functionalization methods in which fluorescence enhancement following reaction of Anth-$N_3$ with DBCO-containing vesicles was used to estimate DBCO-responsive content [28,32]. DBCO-responsive fluorescence in DBCO-treated HEV preparations was evaluated using 9-(azidomethyl) anthracene (Anth-$N_3$). Anth-$N_3$ was synthesized in-house from 9-(chloromethyl)anthracene (Anth-Cl) [33] and characterized as described in SI. A fresh Anth-$N_3$ stock solution was prepared by dissolving 1.8 mg of Anth-$N_3$ in 1.05 mL of anhydrous DMSO and was protected from light. DBCO-treated HEVs were dispersed in PBS. Assay mixtures of each trial were prepared as: duplicate Anth-$N_3$ reagent-control mixtures containing 17.3 µL of Anth-$N_3$ stock solution and 32.6 µL of DMSO; duplicate DBCO-treated HEV assay mixtures containing 25 µL of HEV dispersion, 17.3 µL of Anth-$N_3$ stock solution, and 7.63 µL of DMSO; and duplicate DBCO-treated HEV background controls containing 25 µL of HEV dispersion and 25 µL of DMSO. Each mixture had a final volume of 50 µL. Duplicate technical replicate values were averaged within each experimental trial to obtain a single trial-level value. DMSO was used as the blank. For the controlled lower-feed conditions at pH 7.4 and 8.5, each condition was evaluated in three separate experimental trials. Reported means and standard deviations were calculated from trial-level values. The mixtures were vortexed for 20 s at 1,000 rpm, protected from light, and incubated overnight at 25 °C with orbital agitation. Before fluorescence measurement, reaction mixtures were diluted either tenfold by mixing 10 µL of the reaction mixture with 90 µL of DMSO or 100-fold by mixing 1 µL with 99 µL of DMSO. Fluorescence was measured at excitation and emission wavelengths of 370 and 414 nm, respectively. Fluorescence-enhancement values and apparent DBCO-responsive conversion metrics were calculated according to the procedures described in references [28,32], with the equations and calculation steps provided in SI. Given the application of the Anth-$N_3$ assay to a compositionally complex HEV preparation, the resulting fluorescence-enhancement values were interpreted comparatively across treatment conditions and were not assigned as absolute surface DBCO densities.

### Treatment of BMP4 and BMP4FITC with Azide-PEG$_6$-NHS Ester

Recombinant human BMP4 and BMP4FITC were separately reconstituted according to the respective manufacturers' instructions. For each preparation, 10 µg of protein, corresponding to 20 µL of the reconstituted stock, was diluted with 500 µL of PBS. Azide-PEG$_6$-NHS ester (30 µL of the as-supplied liquid reagent) was added directly to each protein preparation [34,35]. Because density or concentration was not provided for the supplied reagent, the input was defined volumetrically rather than as a molar reagent-to-protein ratio. The reaction pH was adjusted to approximately 8.0–9.0 and monitored during incubation. The mixtures were incubated overnight at 4–8 °C with orbital agitation. Following incubation, the reaction mixtures were dialyzed against 1 L of 0.9% (w/v) sodium chloride at 4–8 °C using a 3.5-kDa MWCO membrane, with three buffer exchanges of approximately 2–4 h each. The recovered preparations are hereafter termed azide-reagent-treated BMP4 and azide-reagent-treated BMP4FITC. This terminology describes the applied reagent-treatment step and does not imply a measured degree of azide substitution. Because NHS ester labeling may occur at multiple accessible primary amines and the degree of azide incorporation was not independently quantified, the recovered protein preparations may contain heterogeneous substitution states.

### Preparation and Purification of BMP4- and BMP4FITC-Associated HEV Preparations

DBCO-treated HEV preparations were separately combined with the corresponding purified azide-reagent-treated BMP4 or BMP4FITC preparations under conditions intended to permit SPAAC (Figure 1) [28,34]. The recovered intermediate preparations were used for the final incubation; preparation-specific input volumes were not available for all exploratory reactions and therefore are not used to assign an absolute HEV-to-protein reaction stoichiometry. The reaction mixtures were incubated overnight at 4–8 °C with orbital agitation. Following incubation, the BMP4- and BMP4FITC-containing reaction mixtures were dialyzed against 1 L of 0.9% (w/v) sodium chloride at 4–8 °C using a 100-kDa MWCO membrane. Three buffer exchanges were performed, each lasting approximately 2–4 h. Dialysis was used to reduce freely diffusible protein, residual small-molecule reagents, and other low-molecular-weight reaction components while retaining HEV-containing fractions. The recovered preparations were operationally designated HEV-BMP4 and HEV-BMP4FITC based on post-purification protein association. BMP4 content was quantified in the recovered fractions and normalized to HEV particle concentration for comparison among preparations. Absolute input-based recovery and coupling efficiencies were not assigned because complete preparation-specific input and recovery volumes were not available for all exploratory preparations. Intensity-weighted hydrodynamic profiles of the recovered preparations were additionally evaluated by dynamic light scattering (DLS), as described in SI.

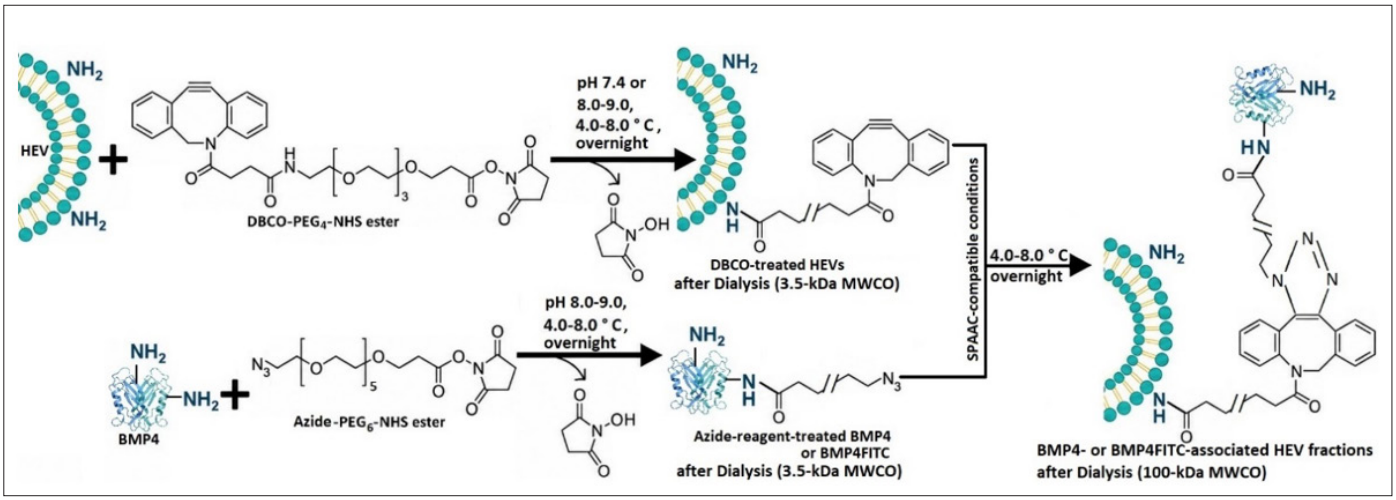



**Figure 1:** Proposed bioorthogonal workflow for preparing BMP4- or BMP4FITC-associated HEVs. Fluorescamine-accessible primary amines in HEV preparations were treated with DBCO-PEG4-NHS ester through an NHS ester–amine reaction, followed by dialysis using a 3.5-kDa MWCO membrane. In parallel, BMP4 or BMP4FITC was treated with azide-PEG6-NHS ester and purified by dialysis using a 3.5-kDa MWCO membrane. The recovered intermediates were then combined under SPAAC-compatible conditions and dialyzed using a 100-kDa MWCO membrane to reduce freely diffusible protein, residual reagents, and other low-molecular-weight components. The resulting preparations were designated BMP4-associated HEVs (HEV-BMP4) or BMP4FITC-associated HEVs (HEV-BMP4FITC). The displayed amine groups, linker attachment sites, and triazole-linked HEV–protein structure are schematic representations of the proposed reaction pathway. They do not specify the number, identity, accessibility, or location of reactive amines; the extent of DBCO or azide incorporation; or the fraction of protein covalently attached through SPAAC

### Quantification of BMP4 in Purified HEV-BMP4 Preparations by ELISA

BMP4 content in purified HEV-BMP4 preparations was measured using the Quantikine Human BMP4 ELISA kit (R&D Systems, Cat. No. DBP400) according to the manufacturer's instructions [36]. A calibration series ranging from 0 to 2,000 pg $mL^{-1}$ was prepared using the supplied recombinant human BMP4 standard and calibrator diluent. Assay diluent RD1-61 (100 µL) was added to each well, followed by 50 µL of standard, control, or undiluted HEV-BMP4 sample. The plate was incubated for 2 h at room temperature and washed four times before addition of 200 µL of the supplied BMP4 conjugate. Following a further 2-h incubation and four additional wash cycles, 200 µL of substrate solution was added, and the plate was incubated for 30 min protected from light. The reaction was stopped by adding 50 µL of stop solution. Absorbance was measured at 450 nm with wavelength correction at 540 nm using a microplate reader. Technical replicate readings were averaged, the response of the zero standard was subtracted, and BMP4 concentrations were calculated from the fitted calibration curve. Matched native-HEV controls, where available, were analyzed and reported separately as assay-background controls; their signals were not subtracted from the HEV-BMP4 concentrations used for particle-normalized calculations. BMP4 content was normalized to the particle concentration of each recovered HEV-BMP4 preparation, as determined by NanoFCM, and reported as picograms of immunoreactive BMP4 per $10^9$ particles. Samples were analyzed without a dedicated vesicle-disruption step. The assay therefore quantified BMP4 that remained immunoreactive and accessible to the ELISA antibodies within the purified HEV-containing preparations. These values were interpreted as particle-normalized, post-purification BMP4 association.

### NanoFCM Analysis of Native and Protein-Associated HEV Preparations

NanoFCM was used for comparative particle-size analysis, particle quantification, and exploratory fluorescence phenotyping of native HEVs and purified HEV-BMP4 or HEV-BMP4FITC preparations. Samples were analyzed using a dual-laser NanoFCM NanoAnalyzer after size calibration with an S16M-Exo silica nanoparticle standard mixture. Particle concentrations and complete-gate size statistics were obtained using consistent calibration and acquisition settings across preparations and were used for particle-normalized downstream analyses. Green (525/40 nm) and far-red (670/30 nm) fluorescence channels were used to detect BMP4FITC- and MemGlow 640-associated fluorescence, respectively [37]. Selected preparations were stained with MemGlow 640, and FITC-A versus PC5-A quadrant gating was used for exploratory fluorescence phenotyping. Detailed acquisition settings, staining conditions, controls, gating procedures, and calculation of FITC-positive events within the MemGlow-positive population are provided in SI.

## Results and Discussion

### Baseline Physicochemical Characterization of Native HEVs

#### NTA of Native HEVs

Across three 60-s technical video acquisitions of the same preparation, the particle-size distribution showed a predominant modal population at 148.0 ± 8.2 nm and a median diameter (D50) of 165.8 ± 8.2 nm (Figure 2a). The corresponding D10 and D90 values were 105.3 ± 9.2 and 293.8 ± 21.4 nm, respectively, while the mean particle diameter was 185.3 ± 10.0 nm. Values are reported as mean ± standard error across the three technical acquisitions. After correction for the experimentally applied dilution factor, the particle concentration of the original purified HEV preparation was estimated as $2.35\times10^{12}\pm4.92\times10^{7}$ particles $mL^{-1}$ (mean ± standard error, n = 3 technical acquisitions). The distribution was predominantly within the nanoscale range but included a smaller contribution from larger light-scattering particles, indicating heterogeneity within the preparation. Because NTA detects and tracks light-scattering particles without independently establishing EV identity, these findings were interpreted together with the TEM observations.

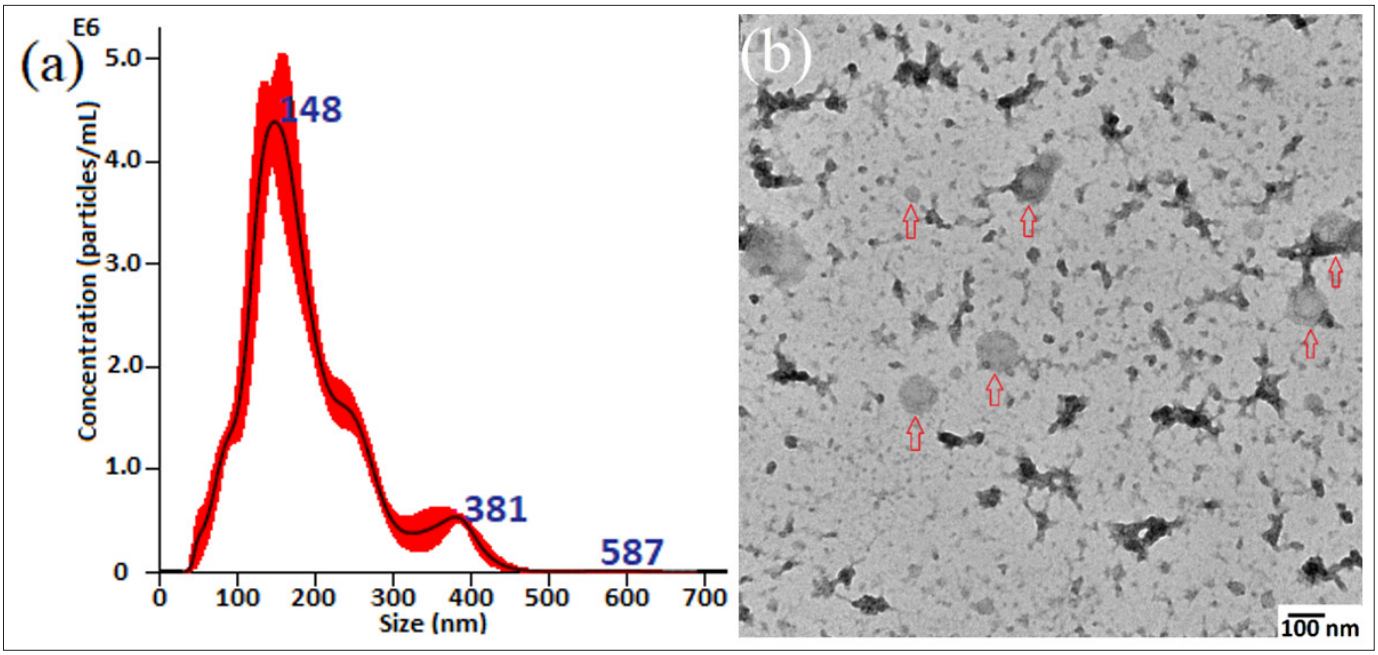



**Figure 2:** Baseline characterization of the purified native HEV preparations: (a) NTA size distribution. The black line represents the mean particle-size distribution obtained from three 60-s technical video acquisitions of the same HEV preparation, and the shaded region represents ±1 standard error across the technical acquisitions. The predominant modal population occurred at approximately 148 nm, with smaller particle populations detected at larger diameters and (b) Representative TEM of the purified native HEV preparation. Red arrows indicate selected nanoscale vesicle-like structures with approximately rounded profiles or discernible membrane-like boundaries. The field also contains smaller electron-dense and irregular structures, illustrating the morphological heterogeneity of the preparation

**TEM of Native HEVs**

TEM revealed a heterogeneous field containing nanoscale vesicle-like structures together with smaller electron-dense features and irregularly shaped material (Figure 2b). Several annotated structures exhibited approximately rounded profiles and discernible membrane-like boundaries, although a clearly resolved bilayer was not uniformly visible. The observed rounded nanoscale structures were broadly consistent with electron-microscopy observations reported for other HEV preparations [19]. Manual measurements of 17 selected vesicle-like structures from multiple TEM micrographs (Figures 2b and S2) yielded a mean apparent diameter of 121.7±46.3 nm, with an observed range of 48.5–240 nm. The TEM measurements likewise showed predominantly nanoscale vesicle-like structures, although direct quantitative comparison with the NTA-derived size distribution was not made because the measurements were obtained from separate HEV batches and by different analytical approaches. Differences between the TEM- and NTA-derived values are expected because conventional negative-stain TEM examines dehydrated, surface-deposited particles and reports projected dimensions, whereas NTA estimates particle size in suspension from Brownian motion and the corresponding hydrodynamic diameter [38–40]. Together with NTA, the TEM observations obtained from separate native HEV batches provide complementary morphological evidence for vesicle-like nanoscale particles in the purified native HEV preparation. However, the images also demonstrate morphological heterogeneity and do not establish that every detected structure represents an intact EV.

**Quantification of Fluorescamine-Accessible Primary Amines in HEV Preparations**

Fluorescamine-accessible primary amines in the native HEV preparation were estimated using 1-hexylamine as the calibration standard [28]. The calibration curve was linear over the working range, with $R^2$=0.9869 at excitation and emission wavelengths of 410 and 470 nm, respectively (Figure S4). The HEV preparation was evaluated without dilution and following 10-fold and 100-fold dilution. The undiluted sample showed a suppressed fluorescence response relative to the calibration range, whereas the response of the 100-fold-diluted sample approached the lower end of the assay range. The 10-fold dilution was therefore selected as the reporting condition because its fluorescence response fell within the usable calibration range and showed a coefficient of variation of approximately 8.2%. This dilution-dependent behavior is consistent with matrix-related effects that may influence fluorogenic amine assays in compositionally complex vesicle preparations, including light scattering, quenching, and differences in accessibility between the calibration standard and HEV-associated primary amines [41–43]. After correction for dilution, the native HEV preparation contained 1.14±0.109 mM 1-hexylamine-equivalent primary amines. Based on the NTA-derived particle concentration of $2.35\times10^{12}$ particles $mL^{-1}$, this corresponded to an estimated $2.92\times10^{5}$ fluorescamine-accessible amine equivalents per particle (Table 1).

**Table 1: Fluorescamine-Accessible Primary Amine Equivalents in the Native HEV Preparation**

| 1-Hexylamine-equivalent amine concentration (mM)[a] | Amine equivalents (mol $mL^{-1}$) | Amine equivalents (molecules $mL^{-1}$) | Native HEV concentration (particles $mL^{-1}$) | Estimated amine equivalents per particle [b] |
|---|---|---|---|---|
| 1.14±0.109 | $1.14\times10^{-6}$ | $6.87\times10^{17}$ | $2.35\times10^{12}$ | $2.92\times10^{5}$ |

[a] Values were derived from the 10-fold-diluted HEV sample and corrected to the original preparation.
[b] Particle normalization used the NTA-derived concentration of the native HEV preparation.

This particle-normalized estimate should be interpreted as a bulk-averaged accessibility metric rather than as an exact molecular count of surface amines on each HEV, because the assay does not distinguish among amines associated with membrane proteins, adsorbed proteins, or other accessible components of the preparation [41–43]. Despite these limitations, the detectable fluorescamine-reactive amine pool provided an experimentally grounded basis for defining nominal DBCO-$PEG_4$-NHS-to-amine feed conditions in subsequent HEV treatment experiments. Similar amine-reactive NHS ester strategies have been used for post-assembly functionalization of vesicles and EV-like systems, although the resulting feed ratios represent reagent-input conditions rather than direct measurements of modification density [28,44,45].

### Treatment of HEVs with DBCO-$PEG_4$-NHS Ester

DBCO-$PEG_4$-NHS ester was used to treat the native HEV preparation through an NHS ester–amine reaction. The NHS ester was selected to react with fluorescamine-accessible primary amines in the HEV preparation, while the DBCO moiety provided the strained-alkyne functionality required for the subsequent azide–alkyne reaction strategy [45,46]. The $PEG_4$ spacer was expected to improve aqueous compatibility and provide separation between the HEV-associated amide linkage and the DBCO group. The treatment conditions were varied to compare the effects of nominal DBCO-to-amine feed ratio and reaction pH. Three exploratory high-feed conditions, corresponding to nominal ratios of approximately 30, 40, and 50, were evaluated at pH 8.0–9.0. A lower nominal ratio of approximately 4.5 was subsequently examined at pH 7.4 and 8.5 (Table 2). All preparations were incubated overnight at 4–8 °C with orbital agitation and purified by dialysis before further analysis. Because matched native-HEV vehicle controls reproducing the preparation-specific DMSO exposure during DBCO-$PEG_4$-NHS treatment were not available, potential vehicle-associated effects on the recovered HEV preparations or DBCO accessibility cannot be excluded.

**Table 2: Experimental Conditions used for Treatment of HEVs with DBCO-$PEG_4$-NHS ester**

| Nominal DBCO-to-amine feed ratio [a] | Reaction pH | Incubation conditions |
|---|---|---|
| ~50 | 8.0–9.0 | Overnight, 4–8 °C, orbital agitation |
| ~40 | 8.0–9.0 | Overnight, 4–8 °C, orbital agitation |
| ~30 | 8.0–9.0 | Overnight, 4–8 °C, orbital agitation |
| ~4.5 | 7.4 | Overnight, 4–8 °C, orbital agitation |
| ~4.5 | 8.5 | Overnight, 4–8 °C, orbital agitation |

[a] Nominal DBCO-to-amine feed ratios were calculated from the amount of DBCO-$PEG_4$-NHS ester added relative to the fluorescamine-derived 1-hexylamine-equivalent amine concentration of the HEV preparation. These values represent reagent-input conditions rather than measured degrees of DBCO incorporation.

The selected reaction matrix enabled comparison of conditions differing in reagent excess and pH-dependent NHS ester reactivity. Mildly basic conditions increase the fraction of unprotonated, nucleophilic primary amines, but increasing pH can also accelerate competing NHS ester hydrolysis [46]. The resulting preparations were therefore evaluated using the Anth-$N_3$ fluorescence assay described in the following section and by downstream BMP4-association measurements. Throughout this study, the recovered products are described as DBCO-treated HEVs, reflecting the applied treatment conditions without assigning an absolute degree of surface modification.

### Comparative Assessment of DBCO-Responsive Fluorescence in Treated HEV Preparations

DBCO-responsive fluorescence in the treated HEV preparations was evaluated using the Anth-$N_3$ assay. Anth-$N_3$ can undergo SPAAC with DBCO-containing species, resulting in fluorescence enhancement relative to the unreacted probe [28,47]. The background-corrected fluorescence-enhancement factor was calculated as:

$$\Omega = \frac{I_{\mathrm{HEV+Anth-N_3}} - I_{\mathrm{HEV\ background}}}{I_0} \qquad (1)$$

where $I_{\mathrm{HEV+Anth\text{-}N3}}$, $I_{\mathrm{HEV\ background}}$, and $I_0$ represent the fluorescence intensities of the Anth-$N_3$-containing HEV mixture, the corresponding HEV background without Anth-$N_3$, and the Anth-$N_3$ reagent control, respectively. Detailed calculation procedures for the apparent DBCO-responsive metrics are provided in SI. Anth-$N_3$ was added in excess relative to the estimated DBCO-responsive content so that probe availability was not expected to limit the assay response. Controlled lower-feed trials were evaluated after 10-fold and 100-fold dilution, whereas exploratory high-feed trials also included 2.5-fold measurements, as detailed in SI. Greater fluorescence enhancement after dilution indicated concentration-dependent optical or matrix effects within the HEV-containing assay mixtures. Comparative calculations were therefore based on measurements falling within the more usable fluorescence-response range. At the lower nominal DBCO-to-amine feed ratio of approximately 4.5, the preparation treated at pH 8.5 produced a larger apparent DBCO-responsive conversion metric than the corresponding preparation treated at pH 7.4. The calculated values were 18.3±2.74% and 13.0±0.64%, respectively (Table 3). The higher response at pH 8.5 is chemically consistent with greater availability of unprotonated primary amines for reaction with the NHS ester, although competing NHS ester

hydrolysis may also increase under more basic conditions [46].

**Table 3: Apparent DBCO-responsive Conversion Metrics for DBCO-treated HEV Preparations**

| Nominal DBCO-to-amine feed condition [a] | Reaction pH | Apparent DBCO-responsive conversion metric |
|---|---|---|
| 30–50 (high feed) | 8.0–9.0 | Approximately 12% in two quantitatively interpretable exploratory trials [b] |
| 4.5 | 7.4 | 13.0±0.64% [c] |
| 4.5 | 8.5 | 18.3±2.74% [c] |

[a] Nominal DBCO-to-amine feed ratios were calculated from the amount of DBCO-PEG4-NHS ester added relative to the fluorescamine-derived 1-hexylamine-equivalent amine concentration.
[b] Only two exploratory high-feed trials met the criteria for quantitative interpretation described in SI.
[c] Values for the nominal ratio of 4.5 are reported as mean ± standard deviation across three separate experimental trials performed under the indicated condition. The reported percentages are comparative metrics derived from the Anth-N3 fluorescence procedure and should not be interpreted as absolute percentages of HEV surface amines converted to DBCO.

The exploratory high-feed preparations generated using nominal DBCO-to-amine ratios of approximately 30–50 at pH values of approximately 8.0–9.0 produced apparent conversion values around 12%. Importantly, the Anth-$N_3$ response did not increase proportionally with increasing DBCO-$PEG_4$-NHS reagent excess. This finding suggests that greater reagent input alone did not improve the detectable DBCO-responsive signal and that reaction pH, NHS ester hydrolysis, matrix effects, and accessibility of HEV-associated amines likely influenced the outcome. At the nominal feed ratio of approximately 4.5, the pH 8.5 condition yielded a larger apparent DBCO-responsive conversion metric than the pH 7.4 condition.

### Treatment of BMP4 and BMP4FITC with Azide-$PEG_6$-NHS Ester

BMP4 and BMP4FITC were treated with azide-$PEG_6$-NHS ester under mildly basic conditions and purified by dialysis before combination with DBCO-treated HEVs. These conditions were selected to permit NHS-ester reaction with solvent-accessible protein amines and thereby generate preparations intended to contain azide-bearing PEG functionalities [46,48]. Because azide incorporation was not independently quantified, no degree of labeling or protein-level azide stoichiometry was assigned. Accordingly, these preparations are operationally designated azide-reagent-treated BMP4 and azide-reagent-treated BMP4FITC. However, NHS ester labeling of proteins can produce heterogeneous substitution states because labeling depends on protein conformation, amine accessibility, reaction pH, reagent hydrolysis, and purification conditions [46,49]. Modification of lysine residues may also affect protein structure or biological activity when functionally important sites are involved [50,51].

### Preparation and Purification of BMP4- and BMP4FITC-Associated HEV Preparations

The purification strategy reduced freely diffusible components but did not provide covalent specificity; therefore, adsorption, aggregation, membrane partitioning, and co-retention remain possible contributors to the measured post-purification BMP4 and BMP4FITC signals. The recovered preparations were operationally designated BMP4-associated HEVs (HEV-BMP4) and BMP4FITC-associated HEVs (HEV-BMP4FITC) based on protein association detected after purification. Related DBCO/azide strategies have been applied to mammalian EVs and other vesicular systems for post-isolation labeling or surface functionalization, supporting the chemical rationale of the present workflow [34,45]. Post-purification BMP4 or BMP4FITC association was subsequently evaluated using ELISA, NanoFCM, and complementary fluorescence measurements. Because the available analytical readouts were designed primarily to compare recovered protein association among treatment conditions, the final preparations are described as protein-associated HEV preparations. Supplementary DLS showed broad, condition-dependent intensity-weighted distributions consistent with formulation heterogeneity; because DLS is strongly influenced by larger scattering species, these data were interpreted as supportive only (Table S1 and Figure S3).

### NanoFCM Particle-Size Distributions of Native and Protein-Associated HEV Preparations

NanoFCM provided internally comparable particle-size estimates for native HEVs and the recovered HEV-BMP4 and HEV-BMP4FITC preparations analyzed using the same calibration and acquisition conditions. All preparations retained predominantly nanoscale event populations, with condition-dependent differences in distribution width and the relative contribution of larger detected events (Table 4 and Figure 3).

**Table 4: NanoFCM-derived Particle-Size Characteristics of Native and Protein-Associated HEV Preparations**

| Preparation | Nominal DBCO-to-amine feed condition | pH | Gated events | Median (nm) | Mean (nm) | SD (nm) |
|---|---|---|---|---|---|---|
| Native HEVs | N/A | N/A | 5,914 | 70.75 | 73.54 | 14.99 |
| HEV-BMP4 | High | 8.0-9.0 | 2,738 | 67.25 | 76.02 | 30.99 |
| HEV-BMP4 | Lower | 7.4 | 3,987 | 68.25 | 73.07 | 22.60 |
| HEV-BMP4 | Lower | 8.5 | 5,825 | 75.75 | 87.49 | 34.16 |
| HEV-BMP4FITC | High | 8.0-9.0 | 3,227 | 81.75 | 94.65 | 32.24 |
| HEV-BMP4FITC | Lower | 7.4 | 6,541 | 69.25 | 72.84 | 19.44 |
| HEV-BMP4FITC | Lower | 8.5 | 5,445 | 76.25 | 87.27 | 32.93 |

Median, mean, and standard deviation values were calculated from the complete gated event population for each NanoFCM measurement. The reported standard deviation describes the within-population dispersion of estimated particle diameters among gated events and does not represent variability among replicate measurements or independently prepared samples. “High” denotes the exploratory high nominal DBCO-to-amine feed condition, whereas “Lower” denotes the nominal feed ratio of approximately 4.5. NanoFCM-derived diameters are calibration-dependent optical estimates and are intended for internal comparison among preparations analyzed under consistent conditions.

Compared with native HEVs, several protein-associated preparations showed greater separation between the median and mean diameters and greater within-population size dispersion, consistent with broader, right-skewed event distributions. For both HEV-BMP4 and HEV-BMP4FITC, the lower-feed preparations generated at pH 8.5 showed larger mean and median diameters than the corresponding preparations generated at pH 7.4. This trend may reflect differences in particle recovery, association of protein-containing material, or the relative abundance of larger particle populations after treatment and purification.

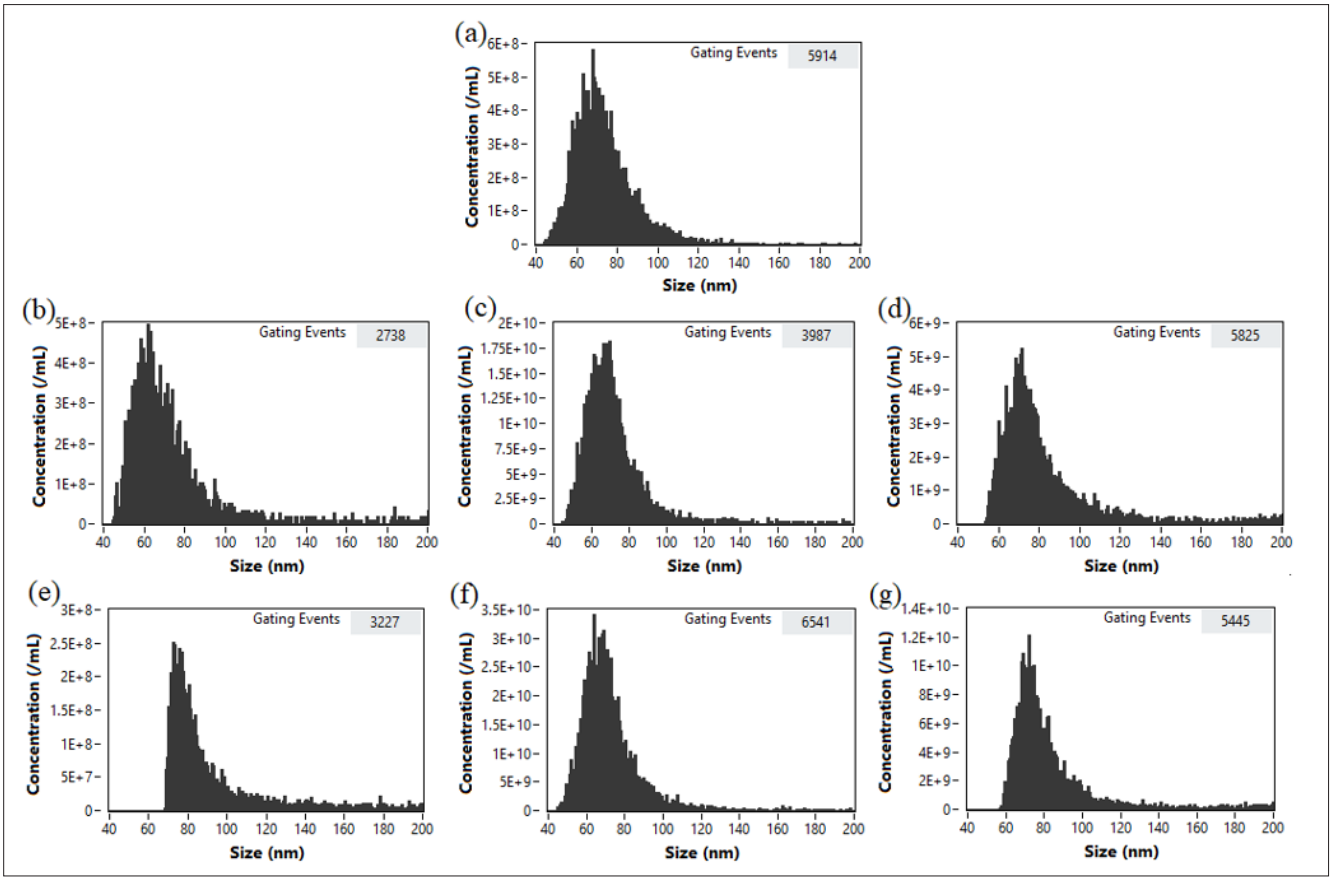



**Figure 3:** NanoFCM-derived particle-size distributions of native and protein-associated HEV preparations: (a) Native HEVs, (b–d) HEV-BMP4 preparations generated under the exploratory high nominal DBCO-to-amine feed condition, the lower nominal feed ratio of approximately 4.5 at pH 7.4, and the lower nominal feed ratio of approximately 4.5 at pH 8.5, respectively, and (e–g) Corresponding HEV-BMP4FITC preparations. Histograms represent the complete gated event population for each preparation and are displayed over the 40–200 nm range for visualization. The concentration-axis scale differs among panels because each distribution is shown using its sample-specific NanoFCM output. Accordingly, comparisons focused on distribution location and shape rather than peak height. Numerical gated-event counts, median diameters, mean diameters, and within-population diameter standard deviations are provided in Table 4

NanoFCM measurements were not obtained for the intermediate DBCO-treated HEV preparations. Therefore, the observed differences between native and final protein-associated preparations cannot be assigned specifically to DBCO treatment, protein incubation, or the final SPAAC-compatible reaction step. The size results were interpreted as comparative characteristics of the recovered particle populations. Because NanoFCM size estimates are derived from calibrated optical-scattering signals and depend partly on particle refractive properties, they were not considered directly interchangeable with NTA-derived hydrodynamic dimensions [52–54]. In addition, the native HEV preparation analyzed by NanoFCM was from a different batch than the preparation characterized by NTA; therefore, the absolute diameters obtained by the two platforms were not interpreted as paired measurements of the same preparation.

**Quantification of BMP4 in Purified BMP4-Associated HEV Preparations**

Immunoreactive BMP4 in the purified HEV-containing preparations was quantified using the Quantikine Human BMP4 ELISA. Native HEVs analyzed under the same assay conditions were included to assess background signal. Because the assay detects antibody-accessible BMP4 in the recovered fractions, the results were interpreted as post-purification BMP4 association. The exploratory high-feed preparations showed relatively low and variable BMP4 recovery, whereas substantially greater BMP4 concentrations were detected under the lower nominal DBCO-to-amine feed ratio of approximately 4.5 (Figure 4 and Table S3). Within the lower-feed comparison, the pH 8.5 preparation showed greater BMP4 recovery than the pH 7.4 preparation. The native-HEV control produced only a low background signal.

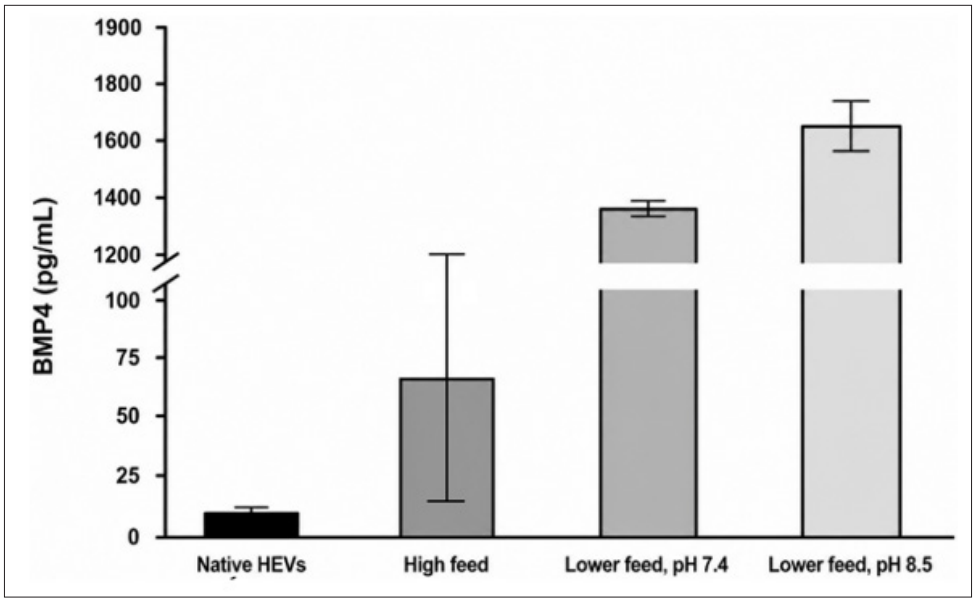



**Figure 4:** Immunoreactive BMP4 concentrations in purified BMP4-associated HEV preparations measured by ELISA. Native HEVs analyzed under the same assay conditions are shown as background controls. "High feed" denotes exploratory preparations generated using nominal DBCO-to-amine feed ratios of approximately 30–50 at pH 8.0–9.0, whereas the lower-feed conditions used a nominal feed ratio of approximately 4.5 at pH 7.4 or 8.5. Displayed summary values are shown as mean ± standard deviation; the experimental basis for each condition, preparation-level values, matched native-HEV backgrounds, and particle-normalized BMP4 contents are provided in Table S3

After normalization to the corresponding NanoFCM particle concentrations, the lower-feed pH 7.4 and pH 8.5 preparations contained approximately 1.60 and 6.66 pg BMP4 per $10^9$ particles, respectively, compared with approximately 0.04–0.60 pg per $10^9$ particles for the exploratory high-feed preparations. These values represent bulk-average immunoreactive BMP4 content in the recovered particle-containing fractions and do not indicate the proportion of individual particles carrying BMP4. For the exploratory high-feed preparations, this range is retained as a descriptive summary of contemporaneous particle-normalized calculations, because the preparations were generated under non-identical nominal feed ratios and pH conditions rather than as a single controlled replicate series. At the treatment-condition level, the ELISA ranking qualitatively paralleled the Anth-$N_3$-responsive results: exploratory high-feed conditions were associated with the lowest particle-normalized BMP4 values, whereas the lower-feed conditions at pH 7.4 and 8.5 showed progressively greater BMP4 recovery. Because neither assay is bond-specific, this qualitative agreement is interpreted only as convergent evidence that the DBCO-$PEG_4$-NHS treatment conditions were associated with subsequent BMP4 recovery. Overall, the lower nominal feed ratio at pH 8.5 produced the greatest particle-normalized BMP4 association among the conditions evaluated. The comparatively lower recovery observed under the exploratory high-feed conditions indicates that greater reagent excess did not proportionally improve protein association.

**NanoFCM Phenotyping of BMP4- and BMP4FITC-Associated HEV Preparations**

NanoFCM was used as an exploratory single-particle phenotyping method to examine MemGlow- and FITC-associated fluorescence in native HEVs and purified HEV-BMP4 or HEV-BMP4FITC preparations. Unstained native HEVs showed minimal PC5-A fluorescence, whereas MemGlow 640 staining produced a distinct PC5-A-positive population, supporting its use as an operational marker of membrane-dye-positive events under the applied acquisition conditions (Figure 5a, b). The HEV-BMP4 preparations showed condition-dependent differences in the relative abundance of MemGlow-positive events (Figure 5c–e). These differences were interpreted descriptively because the preparations differed in treatment condition, recovered particle concentration, and event distribution.

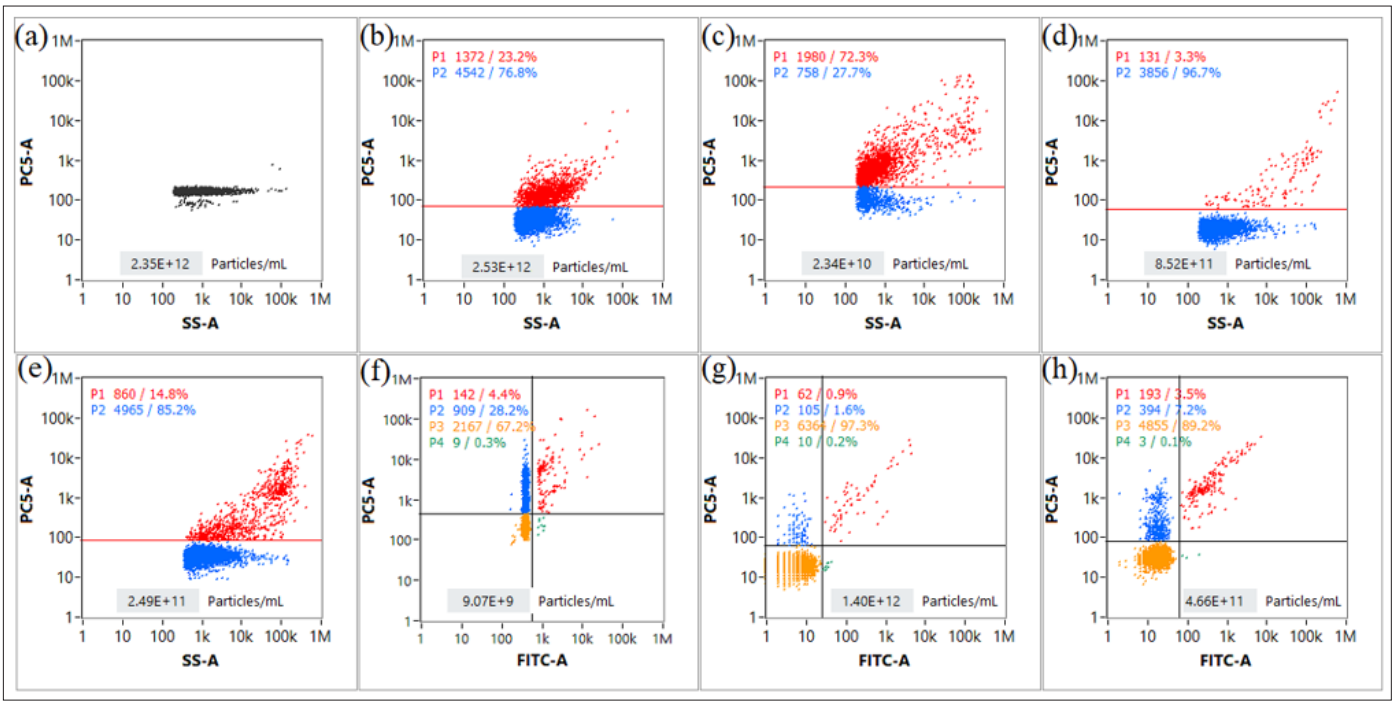



**Figure 5:** NanoFCM phenotyping of native HEVs and purified BMP4- or BMP4FITC-associated HEV preparations: (a) Unstained native HEVs, (b) Native HEVs stained with MemGlow 640. (c–e) PC5-A versus side-scatter plots for HEV-BMP4 preparations generated under the exploratory high-feed condition and the lower-feed conditions at pH 7.4 and 8.5, respectively, and (f–h) FITC-A versus PC5-A quadrant plots for the corresponding HEV-BMP4FITC preparations. P1 represents FITC-positive/MemGlow-positive events, P2 FITC-negative/MemGlow-positive events, P3 FITC-positive/MemGlow-negative events, and P4 events below both fluorescence thresholds. The plotted event populations and quadrant percentages represent exploratory fluorescence-gated phenotyping outputs

For HEV-BMP4FITC preparations, quadrant analysis identified four fluorescence-defined event populations (Figure 5f–h). Detectable FITC fluorescence occurred within subsets of the MemGlow-positive populations under all evaluated conditions (Table 5). However, the condition ranking did not reproduce the ELISA ranking: the lower-feed pH 7.4 preparation showed the largest calculated FITC-positive fraction, whereas the pH 8.5 preparation showed the greatest particle-normalized BMP4 content by ELISA. This difference is consistent with the distinct properties measured by the two methods: ELISA estimates bulk antibody-accessible BMP4, whereas NanoFCM reports the fraction of fluorescence-gated events exceeding instrument-defined thresholds. Overall, the NanoFCM findings provide supportive single-particle-level evidence of BMP4FITC-associated fluorescence within membrane-dye-positive fractions, but they do not independently establish covalent attachment or absolute coupling efficiency. Complementary excitation–emission matrix spectroscopy provided supportive bulk fluorescence characterization and is presented in SI.

**Table 5: NanoFCM-derived FITC-Positive Fractions within MemGlow-Positive Event Populations of Purified HEV-BMP4FITC Preparations**

| Treatment condition | P1: $FITC^+/MemGlow^+$ events | P2: $FITC^-/MemGlow^+$ events | $MemGlow^+$ events, P1 + P2 | $FITC^+$ fraction within $MemGlow^+$ events (%) |
|---|---|---|---|---|
| High feed, pH 8.0–9.0 | 142 | 909 | 1051 | 13.51 |
| Lower feed, pH 7.4 | 62 | 105 | 167 | 37.13 |
| Lower feed, pH 8.5 | 193 | 394 | 587 | 32.88 |

P1 and P2 were defined using FITC-A versus PC5-A quadrant gates. The FITC-positive fraction within the MemGlow-positive population was calculated as [P1/(P1+P2)]×100. Values represent exploratory fluorescence-gated phenotyping metrics rather than absolute fractions of intact HEVs carrying covalently attached BMP4FITC. The lower-feed pH 7.4 result was based on a relatively small MemGlow-positive event population and should be interpreted cautiously.

## Conclusions

This proof-of-concept study evaluates a practical bioorthogonal workflow for preparing BMP4- and BMP4FITC-associated HEV preparations using DBCO/azide chemistry under mild, SPAAC-compatible conditions. Comparison of DBCO-$PEG_4$-NHS treatment conditions showed that the lower nominal DBCO-to-amine feed ratio of 4.5 at pH 8.5 produced the strongest Anth-$N_3$-responsive signal and the highest particle-normalized BMP4 association among the conditions evaluated. Together with NanoFCM detection of BMP4FITC-associated fluorescence within MemGlow-positive event populations, these findings indicate that reaction conditions substantially influenced subsequent protein association and that increasing the nominal DBCO-$PEG_4$-NHS-to-amine feed condition did not necessarily improve the outcome. Together, the Anth-$N_3$, ELISA, NanoFCM, and physicochemical measurements provide a multi-method analytical framework for evaluating chemically treated HEV preparations and their subsequent association with BMP4. Because the current analytical framework was designed primarily for comparative assessment of reaction conditions rather than comprehensive validation of covalent coupling, the recovered materials are conservatively described as BMP4- or BMP4FITC-associated HEV preparations, and no absolute covalent coupling efficiency is assigned. Further studies incorporating direct characterization of protein azide incorporation, matched reaction controls, independently prepared replicate batches, and biological evaluation will allow the chemical and functional aspects of this platform to be defined more comprehensively. Overall, these findings provide a foundation for the continued development of bioorthogonal protein association with PEV preparations and their future evaluation as therapeutic delivery systems.

## Acknowledgment

Article processing charges were provided in part by the UCF College of Graduate Studies Open Access Publishing Fund.

The authors gratefully acknowledge Brent A. Reynolds for his scientific leadership, mentorship, and foundational contributions to this project.

## Author Contributions

**Hamid Moloudian:** Conceptualization, Data curation, formal analysis, investigation, methodology, and Writing– original draft, review and editing.

**Nasser Nassiri Koopaei:** Data curation, formal analysis, methodology

**FNU Joshua:** Data curation, formal analysis, methodology

**Ibrokhim D. Lutfullaev:** Data curation, formal analysis, methodology

**Brent A. Reynolds:** Conceptualization, data curation, formal analysis, funding acquisition, investigation, methodology, project administration, writing - original draft

**Hassan Azari:** Conceptualization, data curation, formal analysis, investigation, methodology, and Writing - review and editing

**Lei Zhai:** Data curation, formal analysis, investigation, methodology, and Writing– review and editing

## Dedication

This article is dedicated to the memory of Brent A. Reynolds, a pioneering neuroscientist and valued mentor, collaborator, and colleague.

## Statements and Declarations

**Ethics Declaration** Not applicable.

**Funding** This work was supported by a grant to Brent A. Reynolds from the Florida Department of Health Live Like Bella® Pediatric Cancer Research Initiative for research on HEV-mediated BMP4 delivery for GBM.

**Data Availability** Additional raw data that remain available can be obtained from the corresponding author upon reasonable request.

**Competing Interests** Nasser Nassiri Koopaei is a co-founder and Chief Executive Officer of EriVan Bio, which supplied the HEV preparations used in this study. Hassan Azari, Nasser Nassiri Koopaei, and the late Brent A. Reynolds are named inventors on U.S. Patent Application US20240024227A1, *Cannabis plant derived extracellular vesicles and therapeutic methods using the same*, which is assigned to the University of Florida Research Foundation, Inc. The remaining authors declare no competing interests.

## References

1. Stupp R, Mason WP, van den Bent MJ, et al. (2005) Radiotherapy plus concomitant and adjuvant temozolomide for glioblastoma. N Engl J Med 352: 987-996.
2. Quail DF, Joyce JA (2017) The microenvironmental landscape of brain tumors. Cancer Cell 31: 326-341.
3. Eder K, Kalman B (2014) Molecular heterogeneity of glioblastoma and its clinical relevance. Pathol Oncol Res 20: 777-787.
4. Pan Y, Jiang Z, Ye Y, et al. (2023) Role and mechanism of BMP4 in regenerative medicine and tissue engineering. Ann Biomed Eng 51: 1374-1389.
5. Piccirillo SGM, Reynolds BA, Zanetti N, et al. (2006) Bone morphogenetic proteins inhibit the tumorigenic potential of human brain tumour-initiating cells. Nature 444: 761-765.
6. Zhou W, Yan K, Xi Q (2023) BMP signaling in cancer stemness and differentiation. Cell Regen 12: 37.
7. Vescovi AL, Galli R, Reynolds BA (2006) Brain tumour stem cells. Nat Rev Cancer 6: 425-436.
8. Rahman M, Azari H, Deleyrolle L, et al. (2013) Controlling tumor invasion: bevacizumab and BMP4 for glioblastoma. Future Oncol 9: 1389-1396.
9. Bos EM, Binda E, Verploegh ISC, et al. (2023) Local delivery of hrBMP4 as an anticancer therapy in patients with recurrent glioblastoma: a first-in-human phase 1 dose escalation trial. Mol Cancer 22: 129.
10. Mehta AM, Sonabend AM, Bruce JN (2017) Convection-enhanced delivery. Neurotherapeutics 14: 358-371.
11. Wang L, Zhang X, Yang Z, et al. (2024) Extracellular vesicles: biological mechanisms and emerging therapeutic opportunities in neurodegenerative diseases. Transl Neurodegener 13: 60.
12. Ramos-Zaldívar HM, Polakovicova I, Salas-Huenuleo E, et al. (2022) Extracellular vesicles through the blood–brain barrier: a review. Fluids Barriers CNS 19: 60.
13. Vahab SA, Vyshma KV, Kumar VS (2025) Exosome-based drug delivery systems for enhanced neurological therapeutics. Drug Deliv Transl Res 15: 1121-1138.
14. Lu X, Fan S, Cao M, et al. (2024) Extracellular vesicles as drug delivery systems in therapeutics: current strategies and future challenges. J Pharm Investig 54: 785-802.
15. Kürtösi B, Kazsoki A, Zelkó R (2024) A systematic review on plant-derived extracellular vesicles as drug delivery systems. Int J Mol Sci 25: 7559.
16. Langellotto MD, Rassu G, Serri C, et al. (2025) Plant-derived extracellular vesicles: a synergetic combination of a drug delivery system and a source of natural bioactive compounds.

Drug Deliv Transl Res 15: 831-845.
17. Karamanidou T, Tsouknidas A (2022) Plant-derived extracellular vesicles as therapeutic nanocarriers. Int J Mol Sci 23: 191.
18. Zeng YB, Deng X, Shen LS, et al. (2024) Advances in plant-derived extracellular vesicles: isolation, composition, and biological functions. Food Funct 15: 11319-11341.
19. Tajik T, Baghaei K, Moghadam VE, Farrokhi N, Salami SA (2022) Extracellular vesicles of Cannabis with high CBD content induce anticancer signaling in human hepatocellular carcinoma. Biomed Pharmacother 152: 113209.
20. Eom JY, Choi SH, Kim HJ, et al. (2022) Hemp-derived nanovesicles protect leaky gut and liver injury in dextran sodium sulfate-induced colitis. Int J Mol Sci 23: 9955.
21. Azari H, Koopaei NN, Nouri MZ, et al. (2020) DDRE-14. Hemp derived extracellular vesicles (EVs): a potential anti-glioma therapy. Neuro Oncol 22(Suppl 2): ii64.
22. Hong V, Presolski SI, Ma C, Finn MG (2009) Analysis and optimization of copper-catalyzed azide–alkyne cycloaddition for bioconjugation. Angew Chem Int Ed 48: 9879-9883.
23. Pickens CJ, Johnson SN, Pressnall MM, Leon MA, Berkland CJ (2018) Practical considerations, challenges, and limitations of bioconjugation via azide–alkyne cycloaddition. Bioconjug Chem 29: 686-701.
24. Dommerholt J, Rutjes FPJT, van Delft FL (2016) Strain-promoted 1,3-dipolar cycloaddition of cycloalkynes and organic azides. Top Curr Chem (Cham) 374: 16.
25. Hao D, Lu L, Song H, et al. (2022) Engineered extracellular vesicles with high collagen-binding affinity present superior in situ retention and therapeutic efficacy in tissue repair. Theranostics 12: 6021-6037.
26. Xu L, Faruqu FN, Liam-Or R, et al. (2020) Design of experiment (DoE)-driven in vitro and in vivo uptake studies of exosomes for pancreatic cancer delivery enabled by copper-free click chemistry-based labelling. J Extracell Vesicles 9: 1779458.
27. Ruan H, Li Y, Wang C, et al. (2023) Click chemistry extracellular vesicle/peptide/chemokine nanocarriers for treating central nervous system injuries. Acta Pharm Sin B 13: 2202-2218.
28. Gai M, Simon J, Lieberwirth I, Mailänder V, Morsbach S, Landfester K (2020) A bio-orthogonal functionalization strategy for site-specific coupling of antibodies on vesicle surfaces after self-assembly. Polym Chem 11: 527-540.
29. Azari H, Moloudian H, Koopaei N, Sicard R, Ganey TM, Reynolds BA (2026) Hemp-derived extracellular vesicles: a novel frontier in nanomedicine and therapeutics. BioDrugs 40: 197-214.
30. Azari H, Schmittgen TD, Nassiri Koopaei N, Reynolds BA (2024) Cannabis plant derived extracellular vesicles and therapeutic methods using the same. US Patent Application US20240024227A1.
31. Koopaei NN, Schmittgen TD, Reynolds BA, Azari H (2022) Method for isolating extracellular vesicles from human neural stem cells expanded under neurosphere culture. In: Deleyrolle LP (ed) Neural progenitor cells: methods and protocols, 2nd edn. Humana, New York: 87-94.
32. van Dongen SFM, Nallani M, Schoffelen S, Cornelissen JJLM, Nolte RJM, van Hest JCM (2008) A block copolymer for functionalisation of polymersome surfaces. Macromol Rapid Commun 29: 321-325.
33. Frick SU, Domogalla MP, Baier G, et al. (2016) Interleukin-2 functionalized nanocapsules for T cell-based immunotherapy. ACS Nano 10: 9216-9226.
34. Liu X, Gong P, Song P, et al. (2019) Rapid conjugation of nanoparticles, proteins and siRNAs to microbubbles by strain-promoted click chemistry for ultrasound imaging and drug delivery. Polym Chem 10: 705-717.
35. Lu L, Duong VT, Shalash AO, Skwarczynski M, Toth I (2021) Chemical conjugation strategies for the development of protein-based subunit nanovaccines. Vaccines 9: 563.
36. R&D Systems Inc (2021) Human BMP-4 immunoassay: Quantikine ELISA. R&D Systems, Minneapolis.
37. Brealey J, Lees R, Tempest R, et al. (2024) Shining a light on fluorescent EV dyes: evaluating efficacy, specificity and suitability by nano-flow cytometry. J Extracell Biol 3: e70006.
38. Rikkert LG, Nieuwland R, Terstappen L, Coumans FAW (2019) Quality of extracellular vesicle images by transmission electron microscopy is operator and protocol dependent. J Extracell Vesicles 8: 1555419.
39. Vestad B, Llorente A, Neurauter A, et al. (2017) Size and concentration analyses of extracellular vesicles by nanoparticle tracking analysis: a variation study. J Extracell Vesicles 6: 1344087.
40. Bachurski D, Schuldner M, Nguyen P, et al. (2019) Extracellular vesicle measurements with nanoparticle tracking analysis—an accuracy and repeatability comparison between NanoSight NS300 and ZetaView. J Extracell Vesicles 8: 1596016.
41. Felix AM, Toome V, De Bernardo S, Weigele M (1975) Colorimetric amino acid analysis using fluorescamine. Arch Biochem Biophys 168: 601-608.
42. Udenfriend S (1972) Development of a new fluorescent reagent and its application to the automated assay of amino acids and peptides at the picomole level. J Res Natl Bur Stand A Phys Chem 76A: 637-640.
43. Hawkes SP, Meehan TD, Bissell MJ (1976) The use of fluorescamine as a probe for labeling the outer surface of the plasma membrane. Biochem Biophys Res Commun 68: 1226-1233.
44. González MI, González-Arjona M, Santos-Coquillat A, et al. (2021) Covalently labeled fluorescent exosomes for in vitro and in vivo applications. Biomedicines 9: 81.
45. Smyth T, Petrova K, Payton NM, et al. (2014) Surface functionalization of exosomes using click chemistry. Bioconjug Chem 25: 1777-1784.
46. Thermo Fisher Scientific Inc (2022) Bioconjugation and crosslinking technical handbook: reagents for bioconjugation, crosslinking, biotinylation, and modification of proteins and peptides. Thermo Fisher Scientific Inc.
47. Baier G, Siebert JM, Landfester K, Musyanovych A (2012) Surface click reactions on polymeric nanocapsules for versatile functionalization. Macromolecules 45: 3419-3427.
48. Hermanson GT (2013) Bioconjugate techniques, 3rd edn. Academic Press, Amsterdam.
49. Lumiprobe Corporation (n.d.) NHS ester labeling of biomolecules containing primary amino groups. Lumiprobe. Available from: https://www.lumiprobe.com/protocols/nhs-ester-labeling. Accessed 23 Aug 2026.
50. Yamamoto Y, Tsutsumi Y, Yoshioka Y, et al. (2003) Site-specific PEGylation of a lysine-deficient TNF-α with full bioactivity. Nat Biotechnol 21: 546-552.
51. Dozier JK, Distefano MD (2015) Site-specific PEGylation of therapeutic proteins. Int J Mol Sci 16: 25831-25864.
52. Welsh JA, Arkesteijn GJA, Bremer M, et al. (2023) A compendium of single extracellular vesicle flow cytometry. J Extracell Vesicles 12: e12299.
53. van der Pol E, de Rond L, Coumans FAW, et al. (2018) Absolute sizing and label-free identification of extracellular vesicles by flow cytometry. Nanomedicine 14: 801-810.

54. de Rond L, Coumans FAW, Nieuwland R, van Leeuwen TG, van der Pol E (2018) Deriving extracellular vesicle size from scatter intensities measured by flow cytometry. Curr Protoc Cytom 86: e43.

## Supplementary Information (SI)

## Supplementary Materials and Methods

### Additional Materials

Core materials and procedures used for HEV treatment, protein association, and NanoFCM analysis are described in the main manuscript. Additional methodological details and supplementary procedures are provided below.

9-(Chloromethyl)anthracene (Anth-Cl; Fisher Scientific, Cat. No. AC188180025, ≥98%) and sodium azide were used for the synthesis of 9-(azidomethyl)anthracene (Anth-$N_3$). N,N-Dimethylformamide (DMF), chloroform, ethanol, and deionized (DI) water were used as the reaction solvent and during product isolation and purification. The Pierce BCA Protein Assay (Thermo Scientific/Life Technologies, USA) was used to measure BCA-detectable protein in the purified native HEV preparation, and bovine serum albumin (BSA) was used as the calibration standard. Unless otherwise specified, reagents and solvents were of analytical grade and used as received.

### Measurement of BCA-Detectable Protein Content in Purified Native HEVs

The BCA-detectable protein content of the purified native HEV preparation was measured using the Pierce BCA Protein Assay (Thermo Scientific/Life Technologies, USA) according to the manufacturer's microplate protocol and the established bicinchoninic acid method [1]. The HEV suspension was brought to room temperature and diluted in PBS, where necessary, to obtain an absorbance response within the calibration range. BSA standards were prepared in PBS to match the sample buffer matrix. For each measurement, 25 µL of standard or HEV sample was combined with 200 µL of freshly prepared BCA working reagent in a clear, flat-bottom 96-well plate. The working reagent was prepared by mixing Reagents A and B at a 50:1 volume ratio.

The plate was mixed, incubated at 37 °C for 30 min, and cooled to room temperature before absorbance was measured at 562 nm. Blank-corrected absorbance values were used to construct the calibration curve, and the BCA-detectable protein concentration was calculated from the fitted curve and corrected for sample dilution, where applicable. Samples were analyzed without a dedicated vesicle-disruption step. Protein content was normalized to the NTA-derived particle concentration of the native HEV preparation. The BCA result was obtained from a single measurement of one purified native HEV preparation; no technical or independent replicate measurements were performed.

### DLS of HEV Preparations Across Treatment and Preparation Stages

DLS was used as a supplementary method to compare the intensity-weighted hydrodynamic profiles of native HEVs, DBCO-treated HEVs, HEV-BMP4 preparations, and HEV-BMP4FITC preparations. Measurements were performed using a Zetasizer Nano ZS90 instrument (Malvern Panalytical, UK) equipped with a 633-nm helium–neon laser and a 90° detection geometry.

Samples were diluted with PBS, where necessary, to obtain approximately 1 mL of suspension suitable for measurement. The preparations differed in particle concentration, turbidity, and color. Measurements were conducted at room temperature in disposable cuvettes. Three consecutive measurements were acquired for each sample condition in automatic mode and treated as technical measurements of the same preparation. Measurement duration and attenuation were selected automatically by the instrument. Data were processed using Malvern software version 2.1. The Z-average hydrodynamic diameter, polydispersity index, and diameter and relative intensity of the principal intensity-weighted peak were recorded. Numerical parameters are reported as the mean ± standard deviation of the three technical measurements. For graphical presentation, intensity values from the three measurements were averaged at corresponding particle-diameter points to generate one mean intensity-weighted distribution for each preparation. DLS was used to compare bulk hydrodynamic and scattering behavior across preparation conditions. Because intensity-weighted DLS distributions are disproportionately influenced by larger scattering species, the measurements were interpreted as supplementary indicators of formulation heterogeneity.

### Fluorescamine Calibration and Calculation of Accessible Primary Amine Equivalents

A 1-hexylamine stock solution was prepared by diluting 25 µL of 1-hexylamine to a final volume of 15.91 mL with DI water. Calibration standards ranging from 0 to 0.30 mM were prepared from this stock solution, with the 0 mM standard serving as the reagent-background condition. For each standard, 25 µL of 1-hexylamine solution was mixed with 725 µL of 0.1 M borate buffer (pH 9.5) and 250 µL of freshly prepared fluorescamine solution at 0.3 mg $mL^{-1}$ in anhydrous DMSO [2]. The mixtures were vortexed for 30 s, after which 100 µL aliquots were immediately transferred to a clear, flat-bottom 96-well plate. Fluorescence was measured at excitation and emission wavelengths of 410 and 470 nm, respectively. Standards were measured in triplicate as technical replicates, and the relationship between fluorescence intensity and 1-hexylamine concentration was evaluated by linear regression. HEV samples were analyzed under the same reaction conditions, with 25 µL of HEV dispersion replacing the calibration standard. Four independent HEV experimental trials were evaluated, with fluorescence measured in triplicate technical replicates within each trial. Undiluted, 10-fold-diluted, and 100-fold-diluted samples were evaluated to identify a response within the usable calibration range. The 1-hexylamine-equivalent amine concentration was calculated from the fitted regression equation and corrected for sample dilution. The estimated number of fluorescamine-accessible amine equivalents per particle was calculated as:

$$\text{Amine equivalents per particle} = \frac{\left(\frac{F-b}{m}\right) \times DF \times 10^{-6} \times N_A}{C_{\text{particles}}} \quad \text{(S1)}$$

where $F$ is the measured fluorescence intensity, $m$ and $b$ are the slope and intercept of the calibration curve, $DF$ is the sample-dilution factor, $10^{-6}$ converts millimolar concentration (mM) to mol $mL^{-1}$, $N_A$ is Avogadro's constant, and $C_{\text{particles}}$ is the NTA-derived particle concentration in particles $mL^{-1}$.

### Synthesis of Anth-$N_3$

Anth-$N_3$ was synthesized from Anth-Cl in the lab (Figure S1) [3].

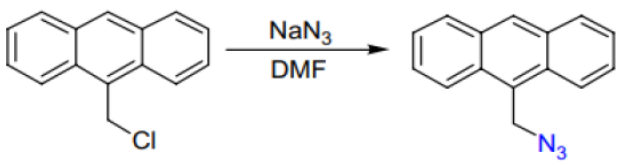



**Figure S1:** Synthesis of Anth-$N_3$ via nucleophilic substitution of 9-(chloromethyl) anthracene with sodium azide ($NaN_3$) in DMF

Briefly, 2.26 g (10 mmol) of Anth-Cl was dissolved in 50 mL of DMF, followed by addition of 1.95 g (30 mmol) of sodium azide. The reaction mixture was heated at 50 °C for 24 h in an oil bath. After completion of the reaction, DMF was removed under reduced pressure using a rotary evaporator. The resulting solid was dissolved in 100 mL of chloroform and washed twice with 150 mL of water to remove water-soluble impurities. The organic phase was separated, and the solvent was removed under reduced pressure. The resulting solid was suspended in ethanol and stirred overnight. The liquid phase was then separated by filtration, cooled first to room temperature and subsequently to 0 °C in an ice bath, resulting in crystallization of yellow needle-like crystals. The crystals were collected and dried under vacuum to obtain purified Anth-$N_3$. The product was characterized by FT-IR, $^1$H-NMR, and $^{13}$C-NMR spectroscopy.

## Calculation of Anth-$N_3$ Fluorescence-Enhancement and Apparent DBCO-Responsive Metrics

Anth-$N_3$ fluorescence was evaluated across separate experimental trials of DBCO-treated HEV assay mixtures following 2.5-fold, 10-fold, and 100-fold dilution. Corresponding HEV-background mixtures without Anth-$N_3$ and Anth-$N_3$ reagent controls without HEVs were analyzed under the same dilution conditions. The background-corrected fluorescence-enhancement factor (Ω) was calculated as defined in the main manuscript. A DMSO-only reading was recorded as a solvent blank. The apparent DBCO-responsive conversion metric was calculated according to the published Anth-$N_3$ fluorescence relationship [2,4]:

$$\text{Apparent DBCO-responsive conversion (\%)} = \frac{\left(\frac{\Omega}{48}\right)\left(\frac{C_{\text{Anth-N}_3} V_{\text{Anth-N}_3} N_A}{C_{\text{particles}} V_{\text{HEV}}}\right)}{N_{\text{amine/particle}}} \times 100 \quad \text{(S2)}$$

where $C_{\text{Anth-N}_3}$ and $V_{\text{Anth-N}_3}$ are the concentration and volume of Anth-$N_3$ added, $N_A$ is Avogadro's constant, $C_{\text{particles}}$ is the particle concentration of the HEV preparation, $V_{\text{HEV}}$ is the volume of HEV dispersion used in the assay, and $N_{\text{amine/particle}}$ is the batch-specific fluorescamine-derived amine-equivalent estimate per particle. The calculations used 7.349 mM Anth-$N_3$, 17.3 µL of Anth-$N_3$ stock, and 25 µL of HEV dispersion. For the HEV batch used in these assays, the particle concentration and fluorescamine-derived amine estimate were $1.5 \times 10^{12}$ particles mL$^{-1}$ and approximately $4.44 \times 10^5$ amine equivalents per particle, respectively. This HEV batch was distinct from the native HEV batch summarized in Table 1 of the main manuscript; therefore, the batch-specific particle concentration and amine-equivalent estimate were used for the Anth-$N_3$ calculations. For the controlled lower-feed comparison at pH 7.4 and 8.5, the 100-fold-diluted measurements were used for the reported apparent conversion metrics because dilution assessment indicated reduced concentration-dependent signal suppression. Exploratory high-feed experiments conducted on different dates were treated as separate exploratory trials rather than as replicate measurements of a single condition. Apparent conversion estimates were assigned only to trials with complete calculation inputs and internally consistent values that remained within the fluorescamine-derived amine-equivalent capacity. The resulting percentages were interpreted as comparative apparent DBCO-responsive metrics. For each experimental trial, duplicate technical measurements of the HEV–Anth-$N_3$ assay mixture, reagent control, and HEV-background control were averaged separately. A trial-level apparent conversion metric was then calculated from those averaged values. The reported mean ± standard deviation was calculated across the three trial-level metrics.

## Calculation of ELISA-Derived Particle-Normalized BMP4 Content

BMP4 concentrations in purified HEV-BMP4 preparations were determined from the fitted ELISA calibration curve after subtraction of the zero-standard response. Technical replicate absorbance readings were averaged before concentration calculation. Matched native-HEV measurements, where available, were reported separately as assay-background controls and were not subtracted from the HEV-BMP4 concentrations used for particle-normalized calculations.

Where applicable, the calculated concentration was corrected using the sample-dilution factor. Particle-normalized BMP4 content was calculated as:

$$\text{BMP4 content}\left(\frac{\text{pg}}{10^9 \text{ particles}}\right) = \frac{C_{\text{BMP4}} \times D}{C_{\text{particles}}} \times 10^9 \quad \text{(S3)}$$

where $C_{\text{BMP4}}$ is the ELISA-derived BMP4 concentration in pg mL$^{-1}$, $D$ is the sample-dilution factor, and $C_{\text{particles}}$ is the post-purification particle concentration of the corresponding HEV-BMP4 preparation in particles mL$^{-1}$, as determined by NanoFCM. For samples analyzed without dilution, $D = 1$. Samples were analyzed without a dedicated vesicle-disruption step.

Accordingly, the calculated values were reported as particle-normalized, antibody-accessible immunoreactive BMP4 content in the purified HEV-containing preparations.

## NanoFCM Acquisition, MemGlow 640 Staining, and Fluorescence Gating

### Instrument Configuration and Acquisition

NanoFCM measurements were performed using a dual-laser NanoFCM NanoAnalyzer. Instrument size calibration was performed using an S16M-Exo silica nanoparticle standard mixture of defined diameters. Side-scatter signals were collected using the 488-nm laser, while green and far-red fluorescence signals were detected through 525/40-nm and 670/30-nm bandpass channels, respectively. FITC-associated fluorescence was recorded in the green channel, and MemGlow 640-associated fluorescence was recorded in the far-red channel. The side-scatter laser was operated at 6 mW with 10% side-scatter decay. When far-red fluorescence was measured, the 638-nm laser was operated at 20 mW. Sampling pressure was maintained at 1.0 kPa, and data were acquired for 1 min using the small-signal threshold mode. Samples were diluted in PBS, as necessary, to obtain approximately 4,000–10,000 events within the analysis region per minute. Data were processed using NanoFCM Professional software. For each preparation, the software reported the number of events within the complete analysis gate and the median, mean, and standard deviation of the estimated particle diameter for that gated population. The complete gated event population was used for the primary comparison of particle-size distributions among native HEVs and the final HEV-BMP4 and HEV-BMP4FITC preparations. Displayed histograms were limited to 200 nm for visualization, whereas the numerical size statistics were calculated from the complete measured size range. Fluorescence-gating procedures used for exploratory phenotyping are described below.

### MemGlow 640 Staining and Control Conditions

The lyophilized MemGlow 640 probe was reconstituted in anhydrous DMSO to obtain a 20 µM stock solution according to the manufacturer's instructions. A 1 µM working dilution was prepared by combining 1 µL of the 20 µM stock with 19 µL of PBS. A preliminary staining assessment was performed by adding 1, 2, or 3 µL of the working dilution to 5 µL of sample, corresponding to final MemGlow 640 concentrations

of approximately 167, 286, and 375 nM, respectively. Samples were incubated for 1 h at room temperature protected from light and subsequently diluted 10-fold or 100-fold before NanoFCM acquisition. Based on the preliminary assessment, 3 µL of the 1 µM MemGlow 640 working solution was added to 5 µL of sample (final dye concentration approximately 375 nM), followed by a 100-fold dilution before acquisition. This condition was used for the phenotyping measurements reported in the main manuscript. Unstained native HEVs were used to establish background fluorescence and the PC5-A threshold for MemGlow-positive events. Unmodified HEV preparations and MemGlow-stained controls were used to establish the fluorescence thresholds applied during dual-color FITC-A versus PC5-A analysis.

**Dual-Color Gating and Calculation**

FITC-A versus PC5-A quadrant gates were used to classify fluorescence-defined events as follows:

P1: FITC-positive/MemGlow-positive
P2: FITC-negative/MemGlow-positive
P3: FITC-positive/MemGlow-negative
P4: FITC-negative/MemGlow-negative

The proportion of FITC-positive events within the MemGlow-positive population was calculated as:

FITC-positive fraction within MemGlow-positive events

$$= \frac{P1}{P1 + P2} \times 100 \quad \text{(S4)}$$

This calculation was used as a fluorescence-gated phenotyping metric for the HEV-BMP4FITC preparations.

**Excitation–Emission Matrix Spectroscopy and Particle-Normalized Analysis of Native HEVs and HEV-BMP4FITC Preparations**

Native HEVs and a purified HEV-BMP4FITC preparation were analyzed by excitation–emission matrix (EEM) spectroscopy. For each measurement, 10 µL of sample was diluted with 3.0 mL of DI water, corresponding to an approximate 1:300 dilution. The undiluted particle concentrations of the native HEV and HEV-BMP4FITC aliquots used for EEM analysis were $1.74 \times 10^{11}$ and $9.08 \times 10^{9}$ particles $mL^{-1}$, respectively. The corresponding estimated post-dilution concentrations were approximately $5.8 \times 10^{8}$ and $3.0 \times 10^{7}$ particles $mL^{-1}$. EEM spectra were acquired using a Duetta fluorescence and absorbance spectrometer (HORIBA Scientific, Japan), with excitation wavelengths ranging from 250 to 500 nm and emission wavelengths ranging from 300 to 800 nm. The EEM matrices were exported as numerical arrays and processed using Python version 3.11 with the NumPy and Matplotlib libraries. To account for differences in particle concentration between preparations, fluorescence intensities were normalized to $10^8$ particles according to:

$$I_{\mathrm{norm},s}(\lambda_{\mathrm{ex}}, \lambda_{\mathrm{em}}) = \frac{I_{\mathrm{raw},s}(\lambda_{\mathrm{ex}}, \lambda_{\mathrm{em}})}{C_s/10^8} \quad \text{(S5)}$$

where $I_{raw,S}$ is the measured EEM intensity for sample $s$, and $Cs$ is the corresponding estimated post-dilution particle concentration in particles $mL^{-1}$. Normalized intensities are therefore expressed as instrument response per $10^8$ particles. For each normalized EEM matrix, the global maximum intensity and its corresponding excitation and emission coordinates were extracted as descriptors of the overall fluorescence profile.

**Supplementary Results**

**TEM**

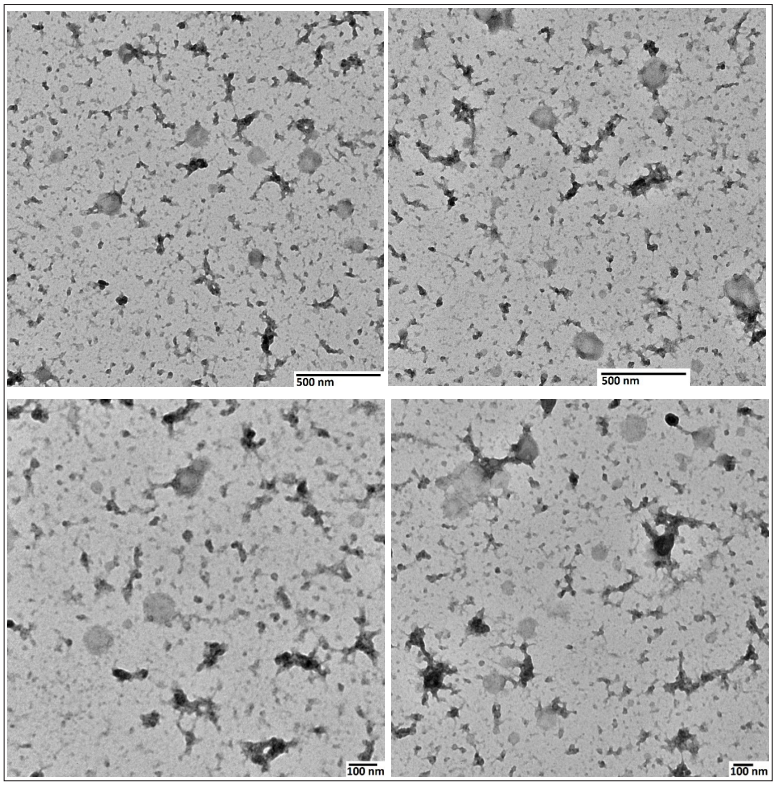



**Figure S2:** Representative TEM micrographs of the purified native HEV preparation. Negatively stained specimens showed a heterogeneous field containing nanoscale, approximately rounded vesicle-like structures together with smaller electron-dense and irregularly shaped material. The images are presented at two magnifications to illustrate both the broader field morphology and selected nanoscale structures. Scale bars: 500 nm in the upper panels and 100 nm in the lower panels.

### BCA-Detectable Protein Content of the Purified HEV Preparation

A single BCA measurement of the purified native HEV preparation yielded approximately 0.75 µg of BCA-detectable protein per 1 × $10^9$ particles. Particle normalization was based on the native-HEV concentration determined by NTA. This value is reported as a particle-normalized characterization parameter rather than as a process-scale extraction yield or a purity measurement. Because the assay was performed on the purified HEV preparation without a dedicated vesicle-lysis step, the detected protein cannot be assigned exclusively to intravesicular or membrane-associated proteins and may include co-isolated proteinaceous material.

### DLS of HEV Preparations Across Treatment and Preparation Stages

DLS revealed broad and condition-dependent intensity-weighted size distributions across native HEVs, DBCO-treated HEVs, BMP4-associated HEV preparations, and BMP4FITC-associated HEV preparations.

**Table S1: Summary of DLS Measurements of HEV Preparations Across Treatment and Preparation Stages**

| Sample | Z-Average (nm) | PDI | Peak 1 (nm) | %Intensity (Peak 1) |
|---|---|---|---|---|
| (a) Native HEVs | 363.5±16.28 | 0.417±0.121 | 483.2±205.1 | 83±25.6 |
| (b) DBCO-treated HEVs (high feed) | 402.7±28.39 | 0.609±0.059 | 444±32.75 | 88.7±1.5 |
| (c) DBCO-treated HEVs (lower feed), pH 7.4 | 830.5±74.19 | 0.386±0.184 | 977.3±153.3 | 93.0±4.3 |
| (d) DBCO-treated HEVs (lower feed), pH 8.5 | 1062±74.67 | 0.5±0.119 | 819.7±195.2 | 100±0 |
| (e) BMP4-associated HEVs (high feed) | 440±23.79 | 0.562±0.033 | 435.2±44.14 | 95.1±4.3 |
| (f) BMP4-associated HEVs (lower feed), pH 7.4 | 602.9±40.84 | 0.585±0.073 | 625.1±129.9 | 91.2±8.4 |
| (g) BMP4-associated HEVs (lower feed), pH 8.5 | 670.8±80.38 | 0.737±0.043 | 714.0±177.1 | 86.5±1.5 |
| (h) BMP4FITC-associated HEVs (high feed) | 294.9±56.19 | 0.643±0.021 | 310.5±39.08 | 68.6±5.7 |
| (i) BMP4FITC-associated HEVs (lower feed), pH 7.4 | 614.9±41.81 | 0.446±0.094 | 726.2±201.9 | 83.9±16.8 |
| (j) BMP4FITC-associated HEVs (lower feed), pH 8.5 | 946.9±50.01 | 0.47±0.05 | 1094.0±68.3 | 93.3±4.5 |

Values represent the mean ± standard deviation of three consecutive technical measurements for each sample condition. High feed denotes the exploratory high nominal DBCO-to-amine feed condition, whereas 'lower feed' denotes the nominal DBCO-to-amine feed ratio of approximately 4.5.

Several conditions showed elevated PDI values and secondary or multimodal populations, indicating formulation heterogeneity and contributions from larger scattering species. Z-average values were generally larger than the sizes obtained by NTA and TEM, which is consistent with the strong intensity weighting of DLS toward larger particles or aggregates. Because all preparations were analyzed using the same DLS platform and acquisition approach, the intensity-weighted profiles were used for relative comparison of bulk scattering behavior across preparation stages despite their limited correspondence with particle-number-based size estimates. These measurements were therefore interpreted as comparative indicators of hydrodynamic behavior and heterogeneity rather than as definitive particle-size measurements or direct evidence of chemical functionalization.

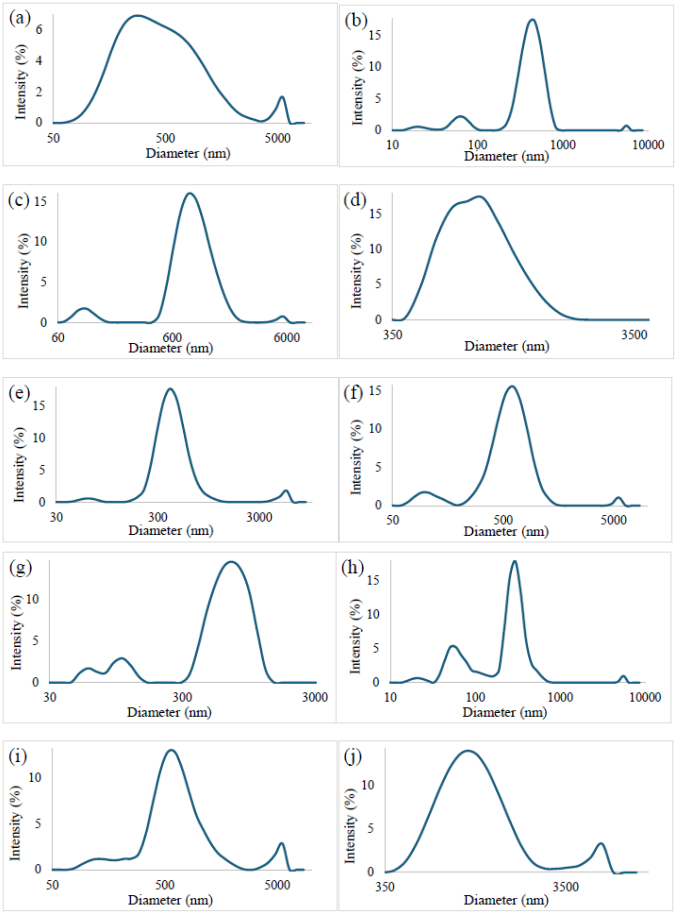



**Figure S3:** Intensity-weighted DLS distributions of HEV preparations across treatment and preparation stages. Distributions are shown for: (a) native HEVs, (b) DBCO-treated HEVs under the high DBCO-to-amine feed condition, (c, d) DBCO-treated HEVs under the lower feed condition at pH 7.4 and 8.5, respectively, (e) BMP4-associated HEVs under the high-feed condition, (f, g) BMP4-associated HEVs under the lower-feed condition at pH 7.4 and 8.5, respectively, (h) BMP4FITC-associated HEVs under the high-feed condition, and (i, j) BMP4FITC-associated HEVs under the lower-feed condition at pH 7.4 and 8.5, respectively. Curves represent averaged intensity distributions from three consecutive technical measurements. The profiles are presented as supplementary comparisons of intensity-weighted hydrodynamic behavior among the preparation conditions

**Fluorescamine Calibration and Dilution Assessment**

The 1-hexylamine calibration curve (Figure S4) was linear over the evaluated range of 0–0.30 mM, yielding

$$F = 139857C + 3101.9;\ R^2 = 0.9869 \qquad \text{(S6)}$$

The undiluted HEV sample showed a suppressed response, whereas the 100-fold-diluted sample approached the lower end of the calibration range. The 10-fold dilution was selected because its response fell within the usable calibration range and showed a coefficient of variation of approximately 8.2% across the four independent trial-level measurements, after averaging the triplicate technical fluorescence readings within each trial.

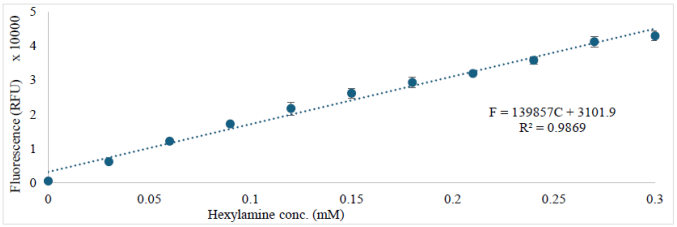



**Figure S4:** 1-Hexylamine calibration curve for the fluorescamine assay. Data points represent mean ± standard deviation of triplicate technical measurements

After correction for dilution, the native HEV preparation contained 1.14 ± 0.109 mM 1-hexylamine-equivalent primary amines, corresponding to approximately $2.92 \times 10^5$ fluorescamine-accessible amine equivalents per particle. The complete particle-normalized calculation is summarized in Table 1 of the main manuscript.

**Synthesis of Anth-$N_3$ from Anth-Cl**

Anth-$N_3$ was successfully synthesized from Anth-Cl via nucleophilic substitution using sodium azide in DMF (Figure S1). The reaction produced bright yellow, needle-like crystalline solids (Figure S5), with an isolated yield of 1.37 g (5.87 mmol, 58.7%) after purification.



**Figure S5:** Synthesized Anth-$N_3$, yellow and needle-shaped crystals

FT-IR spectroscopy supported the conversion of Anth-Cl to Anth-$N_3$ by the appearance of a distinct azide stretching band at approximately 2160–2120 $cm^{-1}$, which was absent in the Anth-Cl precursor (Figure S6). Additional changes in the fingerprint region were consistent with substitution of the chloromethyl group, although this region contains overlapping aromatic and C-Cl-associated vibrations and was therefore treated as supportive evidence.

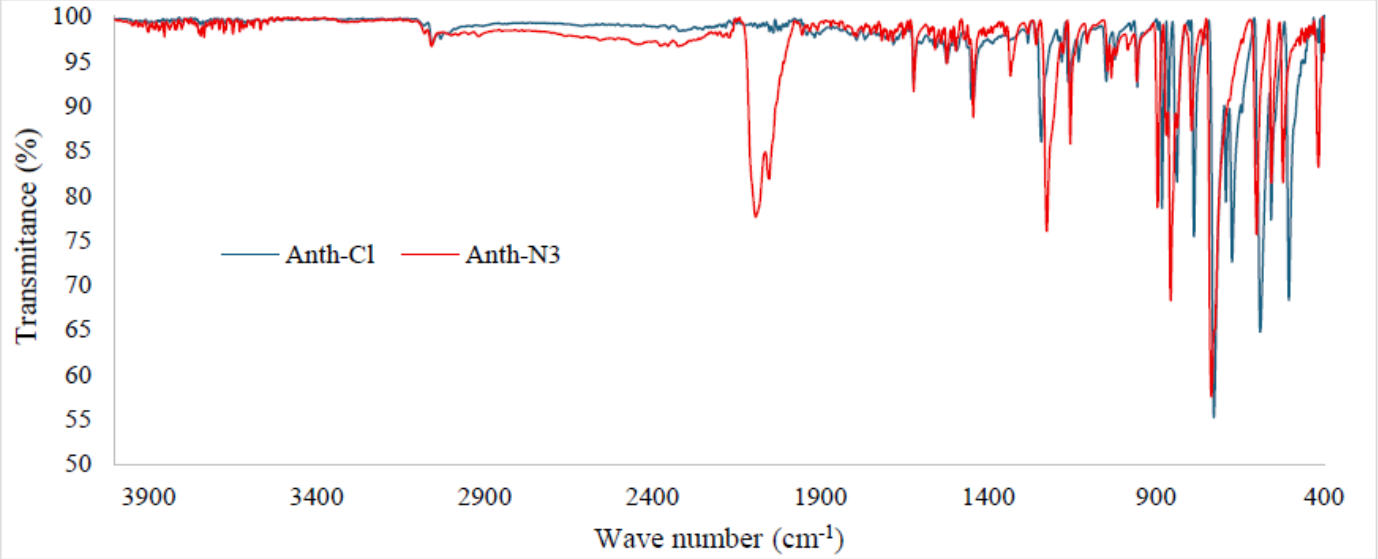



**Figure S6:** FT-IR spectra of Anth-Cl and Anth-$N_3$

The $^1$H-NMR spectrum of the starting material, Anth-Cl, showed a methylene singlet at δ 5.62 ppm. Upon conversion to the azide, this signal shifted upfield to δ 5.34 ppm, consistent with replacement of the chloromethyl functionality by the corresponding azidomethyl group. The aromatic region remained consistent with the expected anthracene backbone (Figure S7).

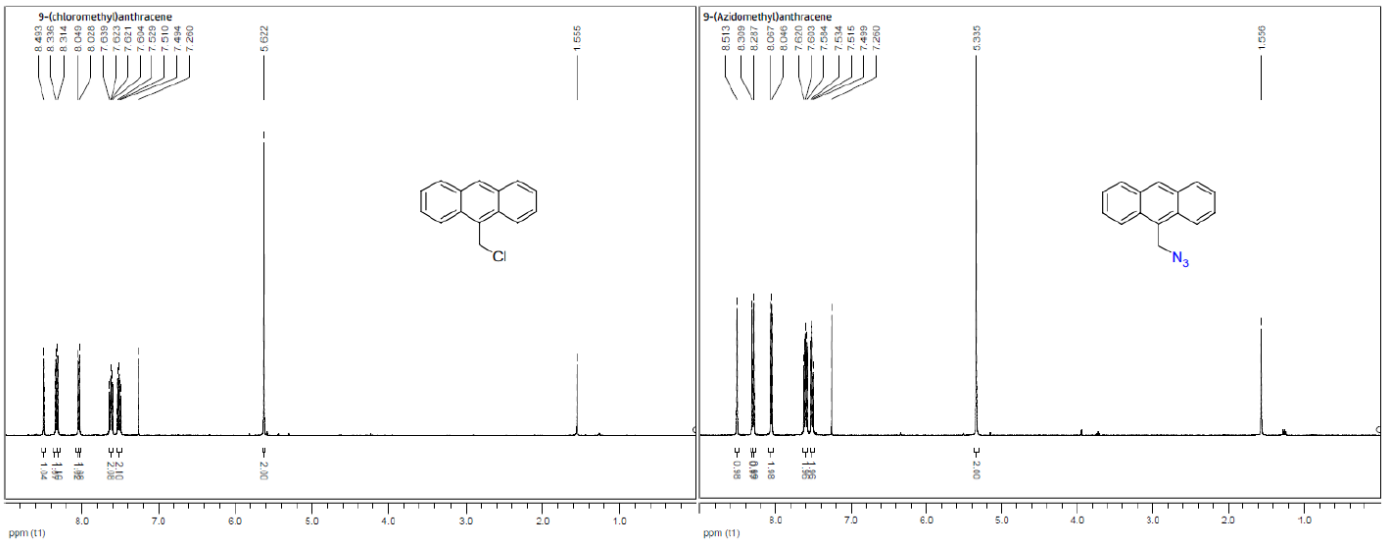



**Figure S7:** The $^1$H-NMR spectra of Anth-Cl (left) and Anth-$N_3$ (right)

The $^{13}$C-NMR spectra (Figure S8) also confirmed the substitution, with the methylene carbon signal shifting from δ 38.96 ppm (-$CH_2$Cl) to δ 46.34 ppm (-$CH_2N_3$) in the azide product. The rest of the aromatic carbon signals remained largely unchanged, supporting selective substitution at the benzylic position.

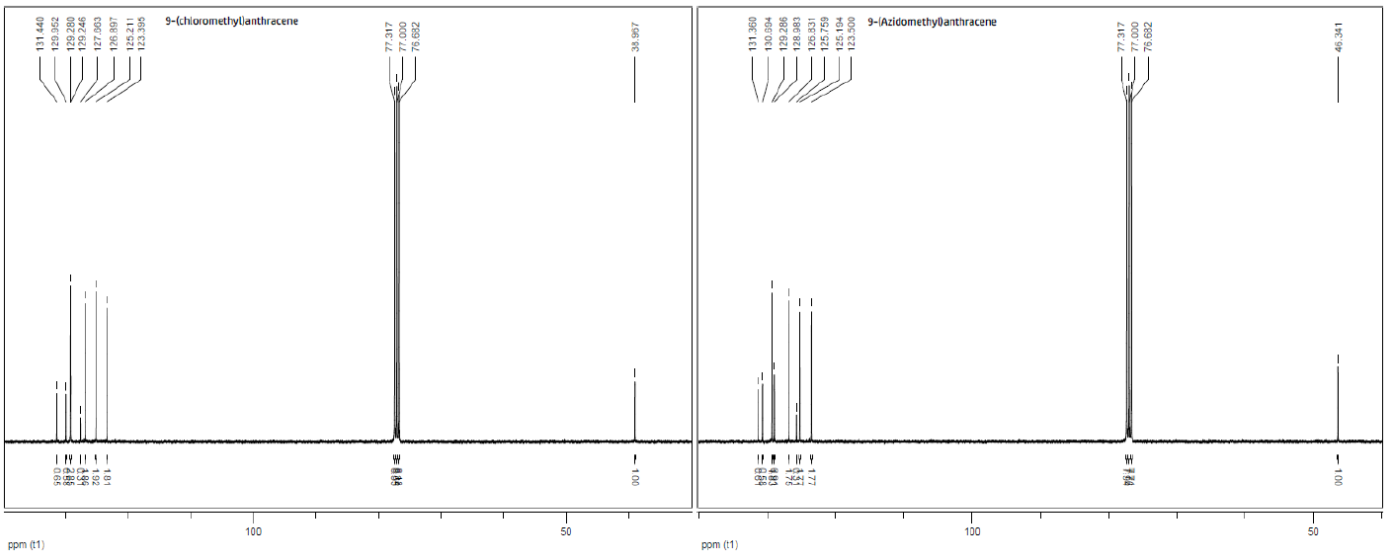



**Figure S8:** The $^{13}$C-NMR spectra of Anth-Cl (left) and Anth-$N_3$ (right)

Together, these data confirm the successful conversion of Anth-Cl to Anth-$N_3$, validating the synthesis and purification procedure.

### Anth-$N_3$ Fluorescence Response and Apparent DBCO-Responsive Metrics

For the controlled lower-feed condition, the background-corrected fluorescence-enhancement factor increased with dilution for both pH values, indicating concentration-dependent optical or matrix effects in the HEV-containing assay mixtures. At each evaluated dilution, the pH 8.5 preparation produced a greater Anth-$N_3$-responsive signal than the corresponding pH 7.4 preparation. The 100-fold-diluted measurements were therefore used for the reported apparent DBCO-responsive metrics because they showed the least evidence of concentration-dependent signal suppression. Using the batch-specific particle concentration and fluorescamine-accessible amine estimate, the lower-feed preparations yielded apparent DBCO-responsive conversion metrics of 13.0 ± 0.64% at pH 7.4 and 18.3 ± 2.74% at pH 8.5 (Table S2).

**Table S2: Quantitatively interpretable Anth-$N_3$ assay outputs for DBCO-treated HEV preparations**

| HEV treatment condition | Measurement basis | Background-corrected Ω | Apparent DBCO-responsive equivalents per particle | Apparent DBCO-responsive conversion metric (%) |
|---|---|---|---|---|
| Exploratory high feed, Trial 1 | Mean of 2.5-, 10-, and 100-fold dilution measurements | 1.224 | $5.20\times10^4$ | 11.7, descriptive |
| Exploratory high feed, Trial 2 | Mean of 2.5- and 10-fold dilution measurements | 1.298 | $5.52\times10^4$ | 12.4, descriptive |
| Lower feed, pH 7.4 | 100-fold dilution | 1.358 | $5.78\times10^4$ | 13.0±0.64 |
| Lower feed, pH 8.5 | 100-fold dilution | 1.915 | $8.15\times10^4$ | 18.3±2.74 |

The exploratory high-feed values represent separate, non-identically prepared trials and are reported descriptively rather than as replicate measurements of a single controlled condition. The 100-fold measurement from exploratory high-feed Trial 2 was excluded because it was identified as an assay error in the original experimental record.

Values for the controlled lower-feed preparations are reported as mean ± standard deviation from three separate experimental HEV–Anth-$N_3$ measurements.

The corresponding apparent DBCO-responsive equivalents in lower feed conditions pH 7.4 and pH 8.5 were approximately $5.78 \times 10^4$ and $8.15 \times 10^4$ per particle, respectively. For these conditions, duplicate technical measurements of the HEV–Anth-$N_3$ assay mixture, reagent control, and HEV-background control were averaged within each trial before calculation of the trial-level apparent DBCO-responsive metric. The exploratory high-feed experiments were conducted as separate trials under non-identical nominal feed ratios and pH conditions. Two trials produced internally consistent responses that remained within the fluorescamine-derived amine-equivalent capacity. These trials yielded descriptive apparent conversion estimates of approximately 11.7% and 12.4%. Other high-feed trials showed pronounced dilution dependence, incomplete batch or reaction metadata, or calculated values exceeding the available amine-equivalent estimate and were therefore retained as qualitative Anth-$N_3$-responsive observations rather than assigned quantitative conversion percentages. Overall, the quantitatively interpretable results showed a descriptive pattern of approximately 12% for the exploratory high-feed trials, 13% for the lower-feed pH 7.4 condition, and 18% for the lower-feed pH 8.5 condition. This trend supports a treatment-dependent change in Anth-$N_3$-responsive fluorescence. Because the assay was applied to a compositionally complex HEV matrix and a native-HEV plus Anth-$N_3$ matrix control was not available, the values were interpreted as comparative apparent DBCO-responsive metrics rather than absolute measurements of surface DBCO density.

**ELISA Calibration and Particle-Normalized BMP4 Content in Purified HEV-BMP4 Preparations**

The BMP4 ELISA calibration curve (Figure S9) showed a linear response over the evaluated range of 0–2,000 pg mL$^{-1}$, with the fitted relationship:

$$OD = 0.0011C + 0.0544;\ R^2 = 0.9971 \qquad \text{(S7)}$$

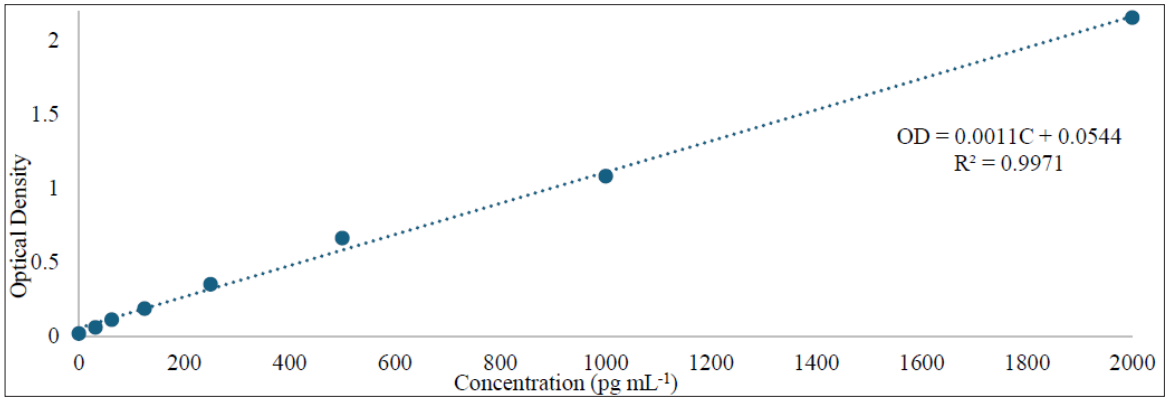



**Figure S9:** BMP4 ELISA calibration curve. Recombinant BMP4 standards ranging from 0 to 2,000 pg mL$^{-1}$ were analyzed using the Quantikine Human BMP4 ELISA. The fitted curve was used to calculate antibody-accessible BMP4 concentrations in purified HEV-BMP4 preparations after correction for the zero-standard response.

This calibration relationship was used to determine antibody-accessible BMP4 concentrations in the purified HEV-BMP4 preparations. The exploratory high-feed preparations showed relatively low and variable BMP4 concentrations after purification. In contrast, substantially greater BMP4 concentrations were detected in the lower-feed preparations generated at pH 7.4 and 8.5, with the pH 8.5 preparation showing the greatest recovered BMP4 concentration (Table S3).

**Table S3: ELISA-derived BMP4 Concentrations and Particle-Normalized BMP4 content in purified HEV-BMP4 Preparations**

| Nominal DBCO-to-amine feed condition | Reaction pH | ELISA-derived BMP4 concentration (pg mL$^{-1}$) [a,b] | Matched native-HEV background (pg BMP4 mL$^{-1}$) [b] | Particle concentration (particles mL$^{-1}$) | Particle-normalized BMP4 content (pg per $10^9$ particles) [d] |
|---|---|---|---|---|---|
| 30–50 [c] | 8.0–9.0 | 59.6 | Not measured | $2.43\times10^{11}$ | 0.04-0.60 |
| | | 137.9 | | $2.43\times10^{11}$ | |
| | | 22.62±5.81 | | $1.57\times10^{11}$ | |
| | | 24.42±11.39 | | $1.0\times10^{12}$ | |
| | | 39.14 | | $1.0\times10^{12}$ | |
| | | 9.19±3.54 | | $1.47\times10^{12}$ | |
| | | 110.25±10.59 | 13.6±6.67 | $1.47\times10^{12}$ | |
| | | 122.1±6.26 | 4.46±1.39 | $1.63\times10^{12}$ | |
| 4.5 | 7.4 | 1366.59±7.73 | 15.61±4.87 | $8.54\times10^{11}$ | 1.60 |
| 4.5 | 8.5 | 1657.18±32.87 | 11.54±3.6 | $2.49\times10^{11}$ | 6.66 |

[a] BMP4 concentrations represent ELISA-derived antibody-accessible BMP4 values after subtraction of the zero-standard response. Matched native-HEV measurements, where available, are reported separately as assay-background controls and were not subtracted from the HEV-BMP4 concentrations used for particle-normalized calculations.

[b] For exploratory high-feed preparations, values reported as mean ± standard deviation reflect technical replicate ELISA measurements within the corresponding preparation. Values reported without an accompanying standard deviation represent individual measurement sets. For the lower-feed pH 7.4 and pH 8.5 conditions, mean ± standard deviation values reflect measurements from three separate HEV-BMP4 preparations generated under the corresponding condition.

[c] The exploratory high-feed preparations were generated using the same general high-feed experimental protocol, with nominal DBCO-to-amine feed conditions spanning approximately 30–50 and reaction pH values spanning 8.0–9.0. These preparations are therefore summarized descriptively rather than treated as a single controlled replicate series.

[d] Particle-normalized BMP4 content was calculated using the corresponding post-purification NanoFCM particle concentration for each preparation. For the exploratory high-feed preparations, the resulting values are summarized descriptively as an approximate range of 0.04–0.60 pg per $10^9$ particles because these experiments were exploratory and were not generated as a single controlled replicate series.

Normalization using the corresponding post-purification NanoFCM particle concentration for each preparation produced the same overall condition pattern. The exploratory high-feed preparations contained approximately 0.04–0.60 pg BMP4 per $10^9$ particles, whereas the lower-feed preparations at pH 7.4 and 8.5 contained approximately 1.60 and 6.66 pg BMP4 per $10^9$ particles, respectively.

These values represent bulk-average, antibody-accessible BMP4 content in the recovered particle-containing preparations and do not indicate the fraction of individual particles carrying BMP4. The greater particle-normalized BMP4 content under the lower-feed pH 8.5 condition was consistent with the condition-dependent Anth-$N_3$-responsive measurements. However, because ELISA is not bond-specific, the results were interpreted as post-purification BMP4 association.

### Excitation–Emission Matrix Analysis of Native HEVs and the HEV-BMP4FITC Preparation

EEM spectroscopy showed distinct bulk fluorescence profiles for native HEVs and the purified HEV-BMP4FITC preparation (Figure S10)

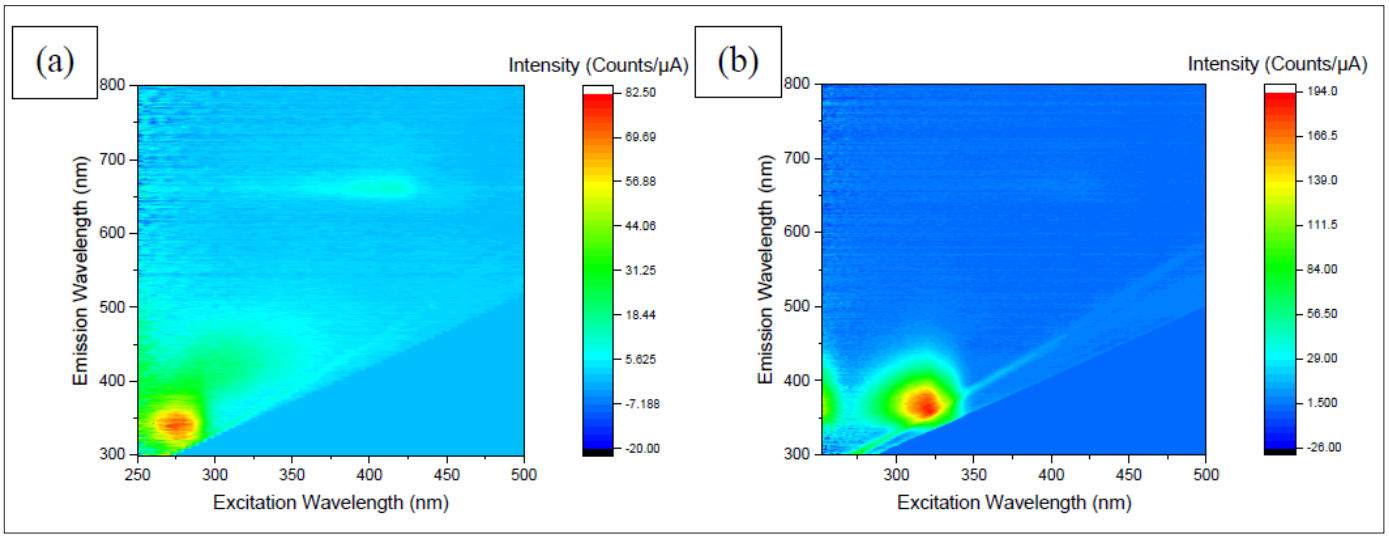



**Figure S10:** EEM fluorescence maps of native HEVs and the purified HEV-BMP4FITC preparation: (a) Native HEVs and (b) the HEV-BMP4FITC preparation were analyzed after dilution of 10 µL of stock preparation into 3.0 mL of DI water. The samples underwent the same volumetric dilution but were not particle matched because their initial particle concentrations differed. Color scales are sample specific and should not be compared directly as equivalent intensity scales.

Because equal sample volumes were diluted rather than particle-matched aliquots, the measured matrices reflected both sample composition and differences in particle concentration. The global fluorescence maxima occurred at different excitation/emission coordinates for the two preparations and outside the characteristic FITC region; they were therefore treated as descriptive features of the complete fluorescence matrices (Table S4).

**Table S4: Descriptive Global EEM Maxima and Particle-Normalized Fluorescence Values for Native HEVs and the HEV-BMP4FITC Preparation**

| Preparation | $\lambda_{ex,max}$ (nm) | $\lambda_{em,max}$ (nm) | Global $I_{max}$ (counts $\mu A^{-1}$) | Estimated post-dilution particle concentration (particles $mL^{-1}$) | Normalized global $I_{max}$ (counts $\mu A^{-1}$ per $10^8$ particles) [a] |
|---|---|---|---|---|---|
| Native HEVs | 270.0 | 342.397 | 82.006 | ($5.8 \times 10^8$) | 14.14 |
| BMP4FITC-associated HEVs | 322.0 | 363.936 | 193.007 | ($3.0 \times 10^7$) | 643.36 |

[a] Fluorescence intensities were normalized to the estimated post-dilution particle concentration and are expressed per $10^8$ particles. The native-HEV sample concentration and the HEV-BMP4FITC concentration were derived from NanoFCM.

After normalization to the estimated post-dilution particle concentrations, the HEV-BMP4FITC preparation showed a greater particle-normalized global maximum intensity than native HEVs. This normalization was used only for descriptive comparison because the particle concentrations were obtained using preparation-specific particle analyses and optical effects may not scale linearly with particle concentration. Overall, the EEM results provide complementary bulk evidence that the recovered HEV-BMP4FITC preparation had a fluorescence profile different from that of native HEVs. However, EEM is an ensemble measurement that may be influenced by endogenous fluorophores, light scattering, inner-filter effects, and other matrix-dependent optical contributions. It cannot distinguish fluorescence from covalently attached BMP4FITC from that of adsorbed, aggregated, or otherwise co-retained fluorescent species. The findings were therefore interpreted as supportive evidence of fluorescent-species enrichment in the purified HEV-containing preparation rather than as a quantitative measurement of covalent coupling.

## References

1. Smith PK, Krohn RI, Hermanson GT, Mallia AK, Gartner FH, Provenzano MD, Fujimoto EK, Goeke NM, Olson BJ, Klenk DC (1985) Measurement of protein using bicinchoninic acid. Anal Biochem 150: 76-85.
2. Gai M, Simon J, Lieberwirth I, Mailänder V, Morsbach S, Landfester K (2020) A bio-orthogonal functionalization strategy for site-specific coupling of antibodies on vesicle surfaces after self-assembly. Polym Chem 11: 527-540.
3. Frick SU, Domogalla MP, Baier G, Wurm FR, Mailänder V, Landfester K, Steinbrink K (2016) Interleukin-2 functionalized nanocapsules for T cell-based immunotherapy. ACS Nano 10: 9216-9226.
4. Lu L, Duong VT, Shalash AO, Skwarczynski M, Toth I (2021) Chemical conjugation strategies for the development of protein-based subunit nanovaccines. Vaccines 9: 563.

**Copyright:** ©2026 Hassan Azari and Lei Zhai, et al. This is an open-access article distributed under the terms of the Creative Commons Attribution License, which permits unrestricted use, distribution, and reproduction in any medium, provided the original author and source are credited.